ImmunoTargets and Therapy

Dovepress
Taylor & Francis Group

Open Access Full Text Article

ORIGINAL RESEARCH

A Novel Prognostic Signature Composed of Autophagy and Liver Metastasis in Colorectal Cancer: Comprehensive Analysis of Bulk and Single-Cell Transcriptomic Data

Binglong Bai[1,*], Yuekai Cui[2,*], Xihao Zhong[1,*], Bingzi Zhu[2], Ziqi Meng[3], Letian Chen[2], Leyan Di[4], Linjing Huang[5], Jisheng Wang[1], Zhouxiang Jin[1], Xufeng Lu[2,6], Bin Zhou[1]

[1]Department of Hepatobiliary and Pancreatic Surgery, the Second Affiliated Hospital and Yuying Children's Hospital of Wenzhou Medical University, Wenzhou, Zhejiang, 325000, People's Republic of China; [2]Department of Gastrointestinal Surgery, the Second Affiliated Hospital and Yuying Children's Hospital of Wenzhou Medical University, Wenzhou, Zhejiang, 325000, People's Republic of China; [3]Department of Anorectal Surgery, the Second Affiliated Hospital and Yuying Children's Hospital of Wenzhou Medical University, Wenzhou, Zhejiang, 325000, People's Republic of China; [4]Wenzhou Medical University, Wenzhou, Zhejiang, 325000, People's Republic of China; [5]Department of Pathology, the Second Affiliated Hospital and Yuying Children's Hospital of Wenzhou Medical University, Wenzhou, Zhejiang, 325000, People's Republic of China; [6]Research Center of Basic Medicine, the Second Affiliated Hospital and Yuying Children's Hospital of Wenzhou Medical University, Wenzhou, Zhejiang, 325000, People's Republic of China

*These authors contributed equally to this work

Correspondence: Bin Zhou; Xufeng Lu, Email pzhoubin@126.com; luxufeng@wmu.edu.cn

ImmunoTargets and Therapy downloaded from https://www.dovepress.com/
For personal use only.

Background: Colorectal cancer (CRC) is a highly aggressive malignancy prone to liver metastasis, which significantly worsens prognosis of patients. Autophagy supports tumor cell survival by meeting metabolic demands and evading programmed cell death. This study aimed to develop a prognostic risk signature for CRC patients by integrating autophagy- and metastasis-related genes and to investigate its association with the tumor immune microenvironment and implications for immunotherapy.

Methods: Weighted gene co-expression network analysis (WGCNA) identified candidate genes related to autophagy and liver metastasis. Univariate Cox and LASSO regression analyses were employed to develop a risk signature in the TCGA cohort, which was subsequently validated using an independent GEO cohort. Functional enrichment, immune infiltration, the heterogeneity and dynamics of macrophages and *CD8*$^+$ T cells, and cell–cell communication were analyzed. The expression patterns of key genes were confirmed through Western blotting and immunohistochemistry.

Results: A prognostic risk signature incorporating six biomarkers (*SPP1*, *JCHAIN*, *DNASE1L3*, *SNAI1*, *TPM1*, and *FKBP10*) was developed and confirmed. The risk signature was an independent prognosticator and outperformed traditional prognostic factors. The patients in high-risk group exhibited heightened Tumor Immune Dysfunction and Exclusion (TIDE) scores, indicating a potential for immunotherapy resistance. Furthermore, enhanced autophagy and metastatic activity were accompanied by differentiation of macrophages toward an *SPP1*$^+$ M2-like phenotype and of *CD8*$^+$ T cells toward an exhausted state. Experimental validation confirmed that *SPP1*, *SNAI1*, and *FKBP10* were highly expressed in CRC tissues.

Conclusion: In our study, we developed and validated a novel autophagy- and liver metastasis-associated prognostic signature for CRC. The risk signature effectively predicts alterations in the tumor immune microenvironment, immunotherapy, chemotherapy sensitivity and intercellular communication across different risk groups. Importantly, our findings reveal that autophagy and liver metastasis synergistically foster an immunosuppressive microenvironment, highlighting a potential target for therapeutic intervention.

Keywords: colorectal cancer, autophagy, liver metastasis, tumor immune microenvironment, cell-cell communication

https://doi.org/10.2147/ITT.S563779
Received: 17 September 2025
Accepted: 13 January 2026
Published: 6 February 2026

© 2026 Bai et al. This work is published and licensed by Dove Medical Press Limited. The full terms of this license are available at https://www.dovepress.com/terms.php and incorporate the Creative Commons Attribution – Non Commercial (unported, v4.0) License (http://creativecommons.org/licenses/by-nc/4.0/). By accessing the work you hereby accept the Terms. Non-commercial uses of the work are permitted without any further permission from Dove Medical Press Limited, provided the work is properly attributed. For permission for commercial use of this work, please see paragraphs 4.2 and 5 of our Terms (https://www.dovepress.com/terms.php).

Introduction

Colorectal cancer (CRC) constitutes a significant global health burden, ranking as the third most common cancer and the second deadliest worldwide currently. Projections indicate a staggering 154,270 newly confirmed diagnoses and 52,900 mortality cases by 2025, necessitating immediate intervention to confront this malignancy's mounting threat.[1] CRC is multifaceted, driven by a combination of genetic susceptibility, demographic factors, lifestyle choices, and dietary patterns.[2] Compounding the issue, the aging global population has intensified the burden of malignant tumors.[3] In spite of advancements in treatments such as surgery, chemotherapy, immunotherapy, and targeted therapies have tremendously improved outcomes for early-stage patients.[4] Nonetheless, the prognosis for advanced CRC patients remains dismal, thereby underlining the dire need for innovative research.

In the realm of CRC treatment, the cancer's stage holds paramount importance, exerting a profound influence on the selection of therapeutic approaches. Around a fifth of patients present with metastasis at their first diagnosis. Survival statistics vary widely. To be specific, stage III patients have a 30–60% 5-year survival rate, but that plummets to a measly 3% for stage IV.[5] Among metastatic cases, 1-, 3-, and 5-year survival rates are 70–75%, 30–35%, and below 20%, respectively.[6,7] Colorectal liver metastases (CRLM), occurring in roughly half of CRC patients, account for nearly two-thirds of CRC fatalities.[8] The survival time of CRLM patients who received active treatment was considerably prolonged.[9–11] Although nearly half of patients derive prolonged survival benefits from surgical intervention, the persistent post-resection relapse rates remain a pressing clinical challenge.[12] This grim prognosis is predominantly attributable to the cancer's aggressiveness, complexity, and the metastasis and recurrence stemming from chemo resistance.[13,14] These underlined the necessity for improved prognostic biomarkers and therapeutic strategies.

Recent research has illuminated the dual role of autophagy in CRC progression.[15,16] Autophagy helps reshape the tumor immune microenvironment and adapt to stress, which exhibits bimodal functionality, initially suppressing neoplastic progression during early oncogenesis yet paradoxically facilitating metastatic dissemination in advanced disease states.[17] Autophagy plays a pivotal role in modulating dynamic cellular motility and orchestrating metastatic potential, epithelial-mesenchymal transition (EMT), and adaptation to hypoxic conditions.[18–21] By regulating these processes, autophagy is enables cancer cells to sustain their energy needs and avoid programmed cell death, thereby promoting the survival and metastasis of CRC cells. Mechanistic insights reveal a key role of autophagy in liver metastasis across gastrointestinal cancers. For instance, Ni et al demonstrated that tumor-associated macrophages boost autophagy via *GDNF-GFRA1* signaling pathway to facilitate hepatic colonization in gastric cancer.[22] Likewise, He et al linked the *TGF-β/TFEB/RAB5A* axis to liver metastasis through *Itgα5β1*-mediated autophagy in pancreatic cancer.[23] In CRC models, *LIMP2* knockdown suppressed autophagy and liver metastasis,[24] whereas *SEC22B* depletion hindered liver metastasis by impairing autophagy flux.[25] Collectively, these findings position autophagy as a central player in CRLM pathogenesis.

To meet the urgent clinical demand for reliable predictive biomarkers, this investigation employed multidimensional transcriptomic approaches integrating single-cell and bulk RNA sequencing analyses to uncover autophagy-related liver metastatic genes in CRC. Using Univariate Cox and least absolute shrinkage and selection operator (LASSO) regression analyses, we constructed and validated a predictive risk stratification model to enhance clinical prognostic accuracy. This model not only facilitates immune subtype classification but also informs individualized treatment strategies. Cell-cell communication exploration further revealed how risk grouping subgroups reshape the tumor immune microenvironment. Our study not only revealed the intricate relationship between autophagy and CRLM but also laid a solid foundation for precision medicine, offering a glimmer of promise for improved survival outcomes and the design of optimized treatment regimens in CRC.

Methods and Materials

Data Acquisition and Processing

With an aim to develop a robust consensus risk signature, we retrieved normalized fragments per kilobase of transcript per million mapped reads (FPKM) data from the TCGA-COAD and TCGA-READ cohorts originated from the TCGA database (https://portal.gdc.cancer.gov/). We merged the TCGA-COAD (420 cases) and TCGA-READ (145 cases) cohorts, forming a training set known as TCGA-CRC (565 cases), after filtering out individuals with insufficient clinical

information. For external validation, paired transcriptomic microarray data and clinical annotations for 177 patients (GSE17536 cohort) were retrieved from the GEO database (https://www.ncbi.nlm.nih.gov/geo/). Supplementary Table 1 offers specific information. Furthermore, for data on CRC liver metastasis, we sourced microarray information for GSE41568 and GSE81558, as well as individual single-cell transcriptomic profiling from GSE245552 and GSE178318, all from the GEO database.

Identification of the Autophagy- and Metastasis-Related Genes

The GeneCards database was adopted to identify autophagy-related genes (ARGs) and metastasis-related genes (MRGs) by searching for the terms "autophagy" and "metastasis". Using the "GSVA" package (version 2.0.5), single-sample gene set enrichment analysis (ssGSEA) was performed to determine the autophagy and metastasis scores for each CRC patient. WGCNA was employed to identify gene modules that exhibited significant correlations with both autophagy and metastasis with the "WGCNA" package (version 1.72-5).

Identification of the Liver Metastasis Related Genes

The single-cell RNA sequencing datasets GSE245552 and GSE178318 were downloaded from the GEO database and processed using "Seurat" package (version 5.2.0). For dataset GSE245552, low-quality cells with fewer than 200 or over 7,500 genes, expressed genes in less than 3 cells, or over 20% of mitochondrial genes, or over 5% of hemoglobin were removed. For dataset GSE178318, low-quality cells with fewer than 300 or over 6000 genes, expressed genes in less than 3 cells, or over 20% of mitochondrial genes, or over 5% of hemoglobin were removed. First, we normalized the datasets using the "NormalizeData" method, and identified the top 2,000 highly variable genes (HVGs) using the "FindVariableFeatures" function. On this basis, we applied the "ScaleData" function to scale the data, reducing discrepancies in gene expression levels and corrected batch effects for dataset integration across different specimens by using the "Harmony" package (version 1.2.1). T-distributed stochastic neighbor embedding (t-SNE) and uniform manifold approximation and projection (UMAP) method were performed to lessen dimensionality. Last but not least, the cluster identities were determined using the "SingleR" package (version 2.6.0). To pinpoint co-expressed genes associated with liver metastasis, WGCNA was employed. Apart from that, differentially expressed genes (DEGs) were identified via cross-dataset comparison of primary tumor and liver metastasis cells using both single-cell and bulk RNA sequencing data.

Identification of DEGs Between Tumor and Adjacent Tissues in CRC

DEGs between tumor and adjacent tissues were identified using the "limma" package (version 3.60.4). The genes were defined as differentially expressed with a $|\log2(\text{fold change})| > 1.0$ with a p-value < 0.05. The volcano plot was generated by using the "gglpot2" package (version 4.0.1).

Development and Validation of a Novel Prognostic Risk Signature

In an effort to construct an innovative prognostic risk signature for predicting overall survival (OS) for CRC patients, we first performed univariate Cox regression analysis to identify genes significantly correlated with survival using the "survminer" package (version 0.4.9). Genes with statistical significance ($p < 0.05$) were subsequently incorporated into a LASSO-penalized combined-variate regression framework via the "glmnet" R package (version 4.1–8) to facilitate feature selection and dimensionality reduction. Each patient's risk score was calculated using the following equation: risk score = Σn (Coefficient × Exp). Based on the optimal cut-off value, CRC patients were stratified into high- and low-risk groups. The Kaplan-Meier (K-M) survival analysis was then employed to compare OS disparities between two risk groups. Moreover, time-dependent receiver operating characteristic (ROC) curves were generated to provide area under curve (AUC) values to assess predictive accuracy with the "timeROC" package (version 0.4). Finally, the reliability of the risk signature was externally validated using an independent GSE17536 dataset.

Development of a Predictive Nomogram

A novel nomogram was developed using the "rms" package (version 6.8–2), integrating the risk score and clinicopathological characteristics comprising gender, age, and tumor stage, to estimate the 1-, 3-, and 5-year survival probabilities in CRC patients. Thereafter, ROC curves were constructed to gauge the discriminatory capacity of the prognostic nomogram. Calibration curves were used to identify discrepancies between the predicted and actual survival probabilities. Decision curve analysis (DCA) was conducted to assess the clinical utility and net benefit of the nomogram with the "dcurves" package (version 0.5.0).

The Functional Enrichment Analyses

To pinpoint the key biological pathways that distinguished across the spectrum of high- and low-risk groups, gene set enrichment analysis (GSEA) was performed using the "clusterProfiler" (version 4.12.6) and "enrichplot" (version 1.24.4) packages. Additionally, we employed gene set variation analysis (GSVA) to analyze how risk scores and prognostic genes correlated with pathways of hallmarks in CRC.

Immunotherapy Response and Chemotherapy Drug Sensitivity Analysis

The Tumor Immune Dysfunction and Exclusion (TIDE) scores for the TCGA-CRC cohort were sourced from the TIDE database (http://tide.dfci.harvard.edu/). A higher TIDE score suggests greater susceptibility to immune evasion, which implied that immunotherapy would be less effective in turn. Furthermore, to understand how different subgroups relate to immunotherapy efficacy, we dug into the expression levels of several immune checkpoint molecules in these two risk subgroups. Using the "oncoPredict" package (version 1.2), we quantified the half-maximal inhibitory concentration (IC50) or each specimen to evaluate the therapeutic potency of cancer-targeting agents. A lower IC50 value indicates higher sensitivity to these drugs.

Exploration of Immune Infiltration and Somatic Mutation Analyses

Cell-type Identification By Estimating Relative Subsets of RNA Transcripts (CIBERSORT) and the ssGSEA algorithm were used to calculate the relative compositions of 22 immune cell subsets and quantify the enrichment scores of immune cell infiltration, respectively. Furthermore, we downloaded single-nucleotide polymorphism (SNP) data and explored genetic mutation profiles between high- and low-risk groups using the "maftools" package (version 2.20.0). The potential correlations between the risk score and tumor mutation burden (TMB) were analyzed using the "survminer" package (version 0.4.9).

Exploration of Cellular Communication and Receptor-Ligand Interaction

To identify shared CellChat objects, the "CellChat" (version 1.6.1) package was used. These objects were then merged using the "mergeCellChat" function, with the "CellChatDB.Human" database as refrence. To identify key ligand-receptor interactions and map gene distribution patterns, we used the "netVisual_diffInteraction" function to analyze and visualize the results.

AUCell Scoring

The AUCell algorithm (version 1.28.0) was used to quantify the relative activity scores of autophagy and metastasis gene sets in individual cells, enabling comparative analysis between primary and metastatic samples as well as across different cell types.

Pseudotime Analysis

To investigate the developmental trajectories and dynamic gene expression changes in macrophages, pseudotime trajectory analysis was performed using the monocle2 R package (version 2.34.0). We used the DDRTree method for dimensionality reduction and ordered cells along the pseudotime trajectory based on their gene expression profiles.

Construction of Co-Expression Network

To investigate the functional relationships among the key genes, a co-expression network based on the expression profiles was constructed in the training set. We calculated pairwise Spearman correlation coefficients for all genes and connected two genes with an edge if their absolute Spearman correlation coefficient exceeded 0.2.

Western Blotting (WB)

In this study, adjacent, tumor, and liver metastasis tissues from nine colon cancer patients at the Second Affiliated Hospital of Wenzhou Medical University were collected (ethical application reference: 2025-K-153-01). An appropriate amount of tissue samples stored in liquid nitrogen was excised and transferred to ice. Lysis buffer (ApexBio, USA) containing protease and phosphatase inhibitors was added to prepare the protein lysate. The mixture was sonicated for 1 minute, followed by complete lysis for 30 minutes. The homogenate was centrifuged at 15,000 g for 15 minutes at 4°C in a pre-cooled centrifuge, and the supernatant was collected. The total protein concentration of the extract was determined. The supernatant was mixed with diluted loading buffer and denatured at 100°C using a metal bath for 10 minutes. Thirty micrograms of protein per lane were loaded onto a pre-cast 15% SDS-PAGE gel (Bio-Rad, USA), and electrophoresis was performed at constant voltage (80V) for 1–2 hours. Proteins were transferred to methanol-preactivated polyvinylidene difluoride (PVDF) membranes (0.22 μm, Millipore, Burlington, MA, USA) using a semi-dry or wet transfer system. The membranes were blocked with 5% skimmed milk in TBST at room temperature for 2 hours with gentle shaking. Membranes were incubated overnight at 4°C with the following primary antibodies diluted in blocking buffer: Rabbit anti-*SPP1* (1:2000, Affinity), Rabbit anti-*SNAI1* (1:2000, Affinity), Rabbit anti-*FKBP10* (1:2000, Bioss), and *β-Actin* (1:5000, Affinity, internal control). The membranes were washed three times with 1× TBST (10 minutes per wash). HRP-conjugated goat anti-rabbit IgG secondary antibody (1:10,000, Thermo Fisher Scientific, Waltham, MA, USA) was applied, and membranes were incubated at room temperature for 2 hours. Chemiluminescent signals were detected using an ECL substrate (Thermo Fisher Scientific) according to the manufacturer's instructions and visualized via autoradiography or imaging systems.

Immunohistochemistry (IHC)

Following xylene-based dewaxing (three washes, 15 min each), tissue sections were rehydrated via sequential immersion in ethanol gradients (100%, 95%, 85%, 75%; 5 min per concentration). For antigen retrieval, slices were boiled in a citrate buffer (pH 6.0) in a microwave oven, maintaining a temperature of at 95 °C for 15 min. After natural cooling, they were rinsed thrice with PBS, followed by blocking endogenous peroxidase with 3% hydrogen peroxide for 25 min and subsequent PBS rinses. Slices were incubated with the primary antibody overnight at 4 °C with the following primary antibodies: Rabbit anti-*SPP1* (1:200, Affinity), Rabbit anti-*SNAI1* (1:200, Affinity), and Rabbit anti-*FKBP10* (1:200, Bioss). After washing with PBS, the slices were treated with an HRP-conjugated secondary antibody (Thermo Fisher Scientific, 1:500 dilution) at room temperature for 50 minutes. Following additional PBS washes, immunostaining was visualized using a DAB chromogen kit and nuclear-contrasted with hematoxylin according to the manufacturer's instructions. Subsequently, processed slides underwent dehydration via an ethanol gradient, were mounted in neutral resin, and prepared for digital scanning and microscopic assessment. Protein expression was assessed by histochemical score (H-Score) based on IHC staining.

Statistical Analysis

In our study, we performed K-M survival analysis, coupled with the Log-rank test to compare the OS of CRC patients between high- and low-risk groups. To ascertain statistically independent predictors bound up with OS, we performed both univariate Cox and LASSO regression analyses. The t-test was utilized to evaluate differences in TMB, drug sensitivity, and TIDE scores between the risk groups. To ensure the robustness of our findings, each analysis was meticulously repeated. All statistical evaluations were executed via R (version 4.4.0), with statistical significance thresholds established at $P < 0.05$ for all inferential analyses.

Results

Identification of Autophagy and Metastasis Related Genes in CRC

The flowchart of this study was illustrated in Scheme 1. Initially, we filtered genes with relevance scores below the median; a total of 4,230 ARGs and 4,885 MRGs were sourced from the GeneCards database (Supplementary Table 2). Simultaneously, the autophagy and metastasis scores for each patient sample were calculated in the TCGA-CRC dataset using ssGSEA. Next, WGCNA was applied to identify co-expressed genes that correlated with the two scores. Subsequent to sample clustering, we excluded five outliers (Figure 1A). During network construction, upon achieving a scale-free topology fit index of 0.85, the soft thresholding parameter β was configured to 10, giving rise to the identification of 15 distinct modules (Figure 1B and C). Moreover, we found five modules: magenta, brown, tan, midnight blue, and turquoise illustrated a correlation exceeding 0.3 for both autophagy and metastasis in CRC (Figure 1D). Ultimately, 6,450 autophagy- and metastasis-related genes from these WGCNA modules were identified for further analysis.

Identification of Liver Metastasis Related Genes in CRC

Liver metastasis considerably increased the mortality rate of CRC patients. To uncover the underlying mechanisms and key drivers of this metastatic process, RNA sequencing methodologies, encompassing bulk and single-cell approaches, were implemented for transcriptional profiling. Using stringent thresholds ($|\log FC| > 1$ and $P < 0.05$ for bulk RNA-seq; $|\log FC| > 0.25$ and $P < 0.05$ for single-cell RNA-seq), we identified DEGs between primary CRC and liver metastasis tissue samples (Supplementary Figure 1A and B). Single-cell transcriptional analysis identified nine cell types in the GSE245552 cohort (Figure 2A) and eight cell types in the GSE178318 cohort (Figure 2C). In addition, WGCNA in the GSE41568 (Figure 2B) and the GSE81558 (Figure 2D) datasets were utilized to identify genes associated with liver metastasis. We also found 311 co-expressed genes related to liver metastasis from the WGCNA analyses. Ultimately, we identified 1,676 DEGs related to liver metastasis. The TCGA cohort analysis revealed 1,562 DEGs between adjacent and tumor tissues (Figure 2E). By cross-referencing these findings with autophagy-, liver metastasis-, and tumor-related gene sets, we narrowed down the list to 48 key genes for further investigation (Figure 2F).

Construction and Validation of a Prognostic Risk Signature

After screening out the 48 consensus genes, a univariate Cox analysis identified 6 genes with prognostic significance (Supplementary Table 3). Subsequently, LASSO regression analysis was applied to find out 6 genes and develop a risk signature incorporating these genes when the partial likelihood deviation reached its minimum, with an optimal lambda value of 0.0039, as illustrated in Figure 3A and B. Lastly, secreted phosphoprotein 1 (*SPP1*), joining chain of multimeric IgA and IgM (*JCHAIN*), deoxyribonuclease 1L3 (*DNASE1L3*), snail family transcriptional repressor 1 (*SNAI1*), tropomyosin 1 (*TPM1*), and *FKBP* prolyl isomerase 10 (*FKBP10*) were selected for the risk model. Next, we calculated individual patient risk scores by weighting the gene transcription and translation of these 6 genes with their respective regression coefficients. The risk signature was built on the following formula: Riskscore = (0.07945359 * Exp*SPP1*) + (−0.0305215 * Exp*JCHAIN*) + (−0.1573357 * Exp*DNASE1L3*) + (0.2397350 * Exp*SNAI1*) + (−0.2977936 * Exp*TPM1*) + (0.0772828 * Exp*FKBP10*). Based on an optimal cutoff point, CRC patients in the TCGA dataset were divided into high- and low-risk groups. K-M survival analysis revealed that patients in the high-risk group had a significantly poorer survival rate than the low-risk group (Figure 3C). Figure 3E illustrated that increasing risk scores correlate with decreased survival rates, unfavorable patient survival status, and upregulated expression levels of the 6 genes. Subsequently, we validated the risk signature in the GSE17536 dataset and found that it demonstrated a similar trend to the training set (Figure 3D–F). The AUC values of the risk signature in the training set were 0.6215, 0.6313, and 0.6715 for 1-, 3-, and 5-year survival, respectively (Figure 3G). Similarly, in the validation set, the AUC values were 0.6449, 0.6224, and 0.6385 (Figure 3H). These results highlighted the robust predictive performance of the risk signature.

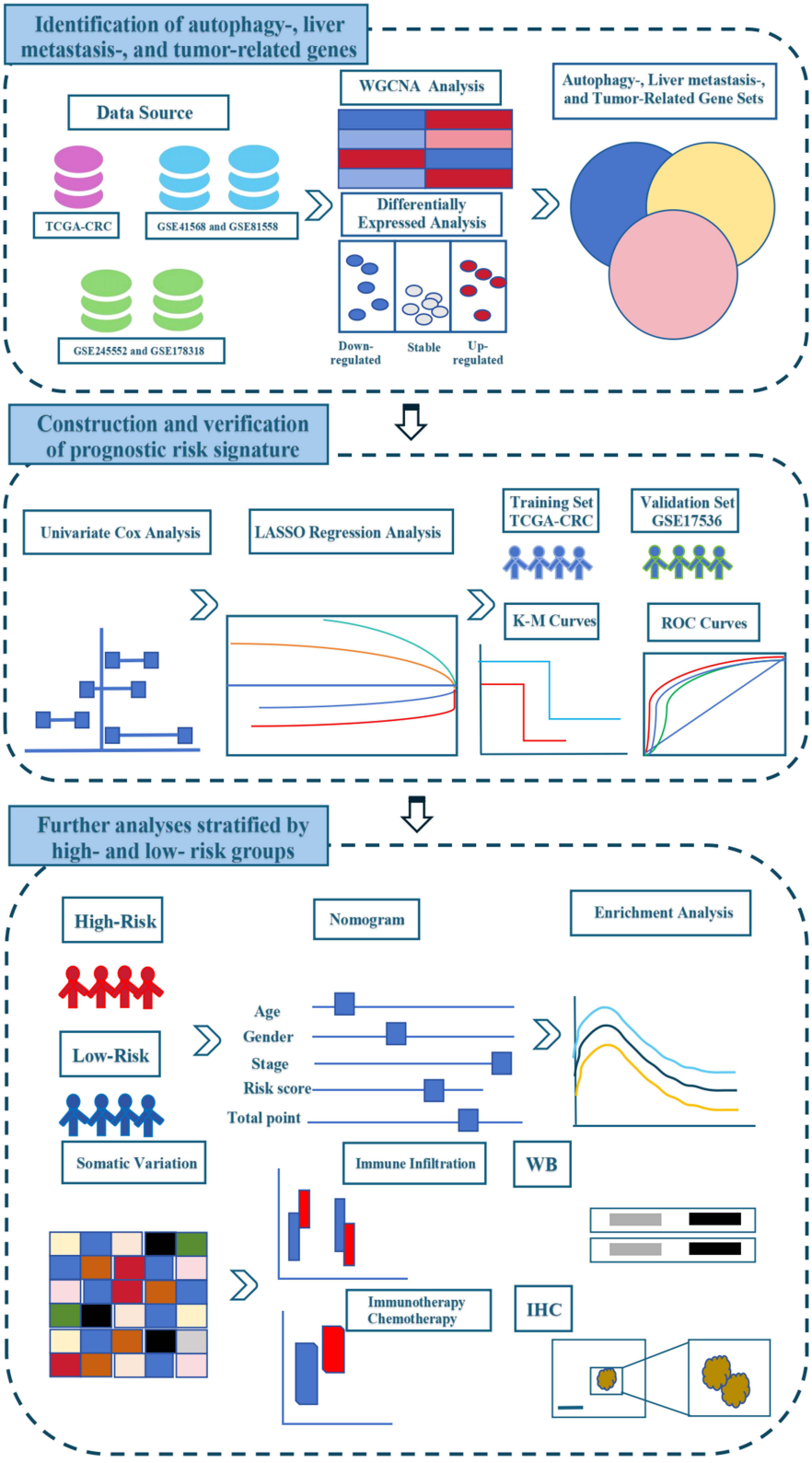

Scheme 1 Flow chart for data collection and analyses in the study.

https://doi.org/10.2147/ITT.S563779

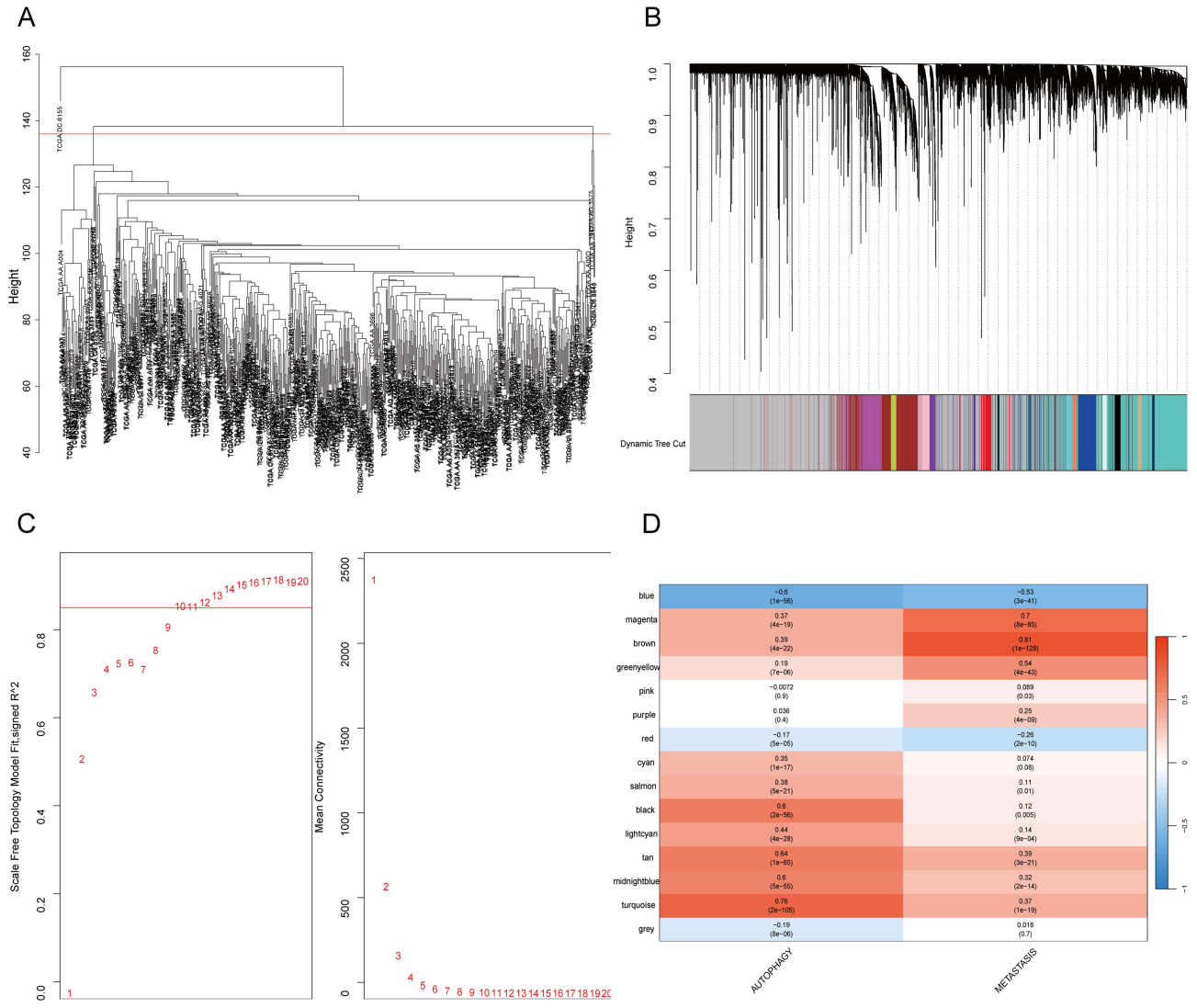

Figure 1 Identification of key autophagy- and metastasis-related genes. (**A**) Sample clustering was performed, and five outlier patients were excluded from the cohort. (**B**) Gene hierarchical clustering tree and color-coded co-expression modules. (**C**) The key parameters of WGCNA. (**D**) WGCNA identified co-expressed gene modules associated with autophagy and metastasis.

Association Between Prognostic Risk Signature and Clinicopathological Characteristics in CRC Patients

In both univariate and multivariate Cox regression analyses, the risk score was identified as a independent prognostic factor for CRC patients in the training (Figure 4A and B) and validation (Figure 4C and D) sets. The AUC values for the risk score, tumor stage, age, and gender were notably 0.657, 0.695, 0.608, and 0.5011, respectively, as detailed in Figure 4E. By stratifying CRC patients according to clinicopathological characteristics, the study confirmed the prognostic predictive ability of the risk signature across different clinical subgroups. As illustrated by the research findings, the risk signature consistently predicted prognosis with high accuracy regardless of ages, genders, stages in the training set (Figure 4F–K) and validation set (Supplementary Figure 2A–F). Additionally, the strip chart demonstrated conspicuous discrepancies in survival status and tumor stage between high- and low-risk groups, as depicted in Supplementary Figure 2G. These insights imply a link between these risk indicators and the progression of CRC in patients.

To enhance clinical utility, a nomogram was developed to integrate clinicopathological characteristics and risk score (Figure 5A). The predictive power was further validated through ROC curves, with AUCs calculated at 1-, 3-, and 5-

 https://doi.org/10.2147/ITT.S563779

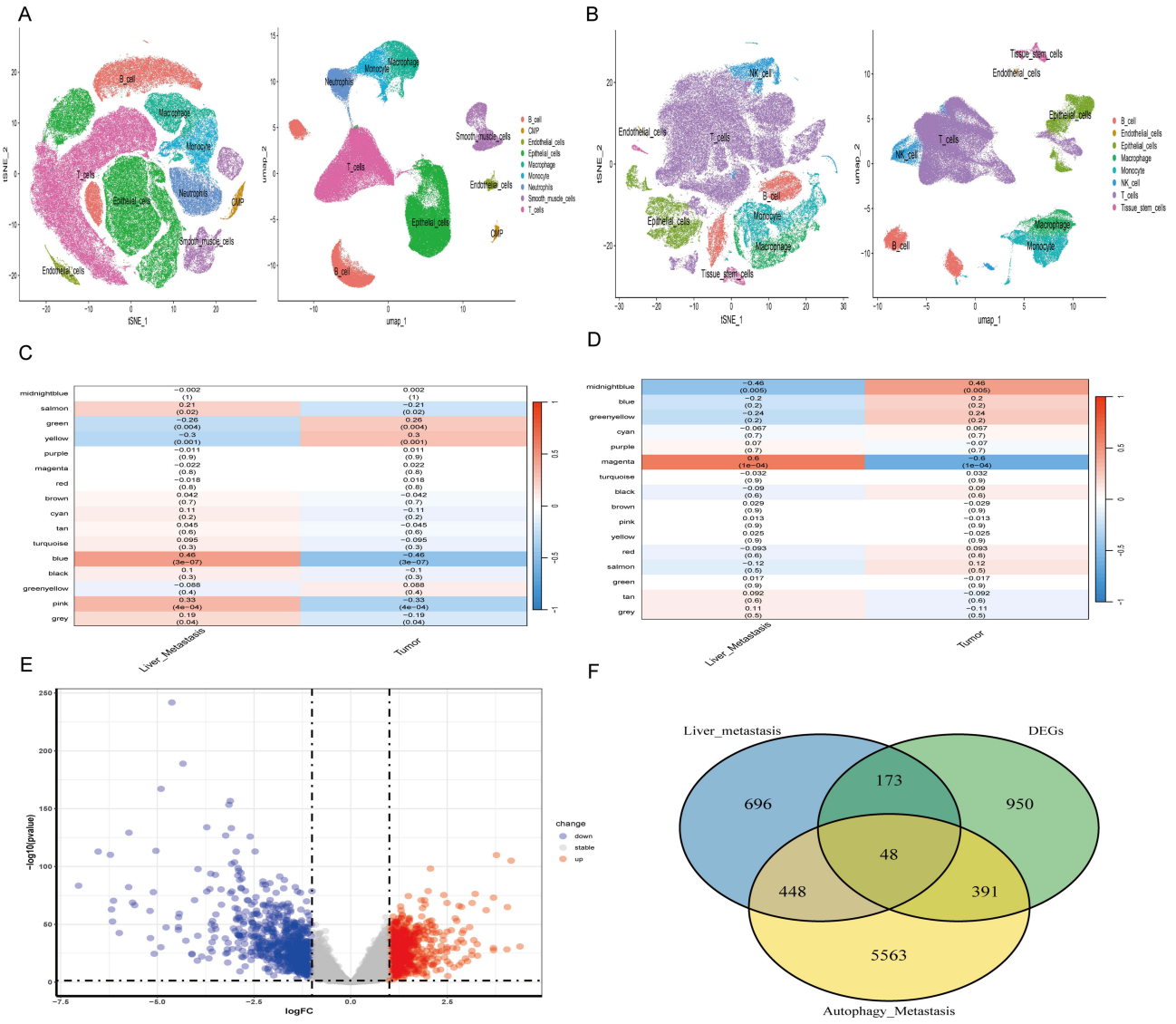

Figure 2 Identification of key autophagy-, liver metastasis-, and tumor-related genes. (**A**) Classification and annotation of cell subgroups in the GSE245552 dataset. (**B**) WGCNA identified gene modules associated with liver metastasis in the GSE41568 dataset. (**C**) Classification and annotation of cell subgroups in the GSE178318 dataset. (**D**) WGCNA identified gene modules associated with liver metastasis in the GSE81558 dataset. (**E**) Differential expression analysis between tumor and adjacent tissues in the TCGA cohort. (**F**) The Venn diagram illustrated 48 key overlapping genes.

years (Figure 5B).The calibration curves of the risk score for 1-, 3- and 5-year suggest that the nomogram is robust in predicting OS (Figure 5C). As illustrated by the decision curve analysis (DCA), the nomogram provided significant clinical benefit (Figure 5D), while the ROC curve for the nomogram illustrated a respectable AUC value of 0.7652 in predicting OS (Figure 5E). Taken together, these findings suggest that this nomogram is robust, reliable, and clinically applicable across diverse patient subgroups.

The Functional Enrichment Analyses Between High- and Low-Risk Groups

GSEA was employed to identify pathway variations between high- and low-risk groups. As depicted by the results, focal ECM-receptor interaction, cytoskeleton in muscle cells, and malaria pathways were enriched in the high-risk group, while sulfur metabolism, nitrogen metabolism and ascorbate and aldarate metabolism were enriched in the low-risk group (Figure 6A and B). In addition, the high-risk group was enriched for the JAK-STAT, MAPK, PI3K-Akt, Rap1 and Wnt pathways, which suggesting that the high-risk group was associated with the progression of CRC (Supplementary Figure 3). Apart from that, we found a strong link between the high-risk group and multiple immune-related gene sets, including

https://doi.org/10.2147/ITT.S563779

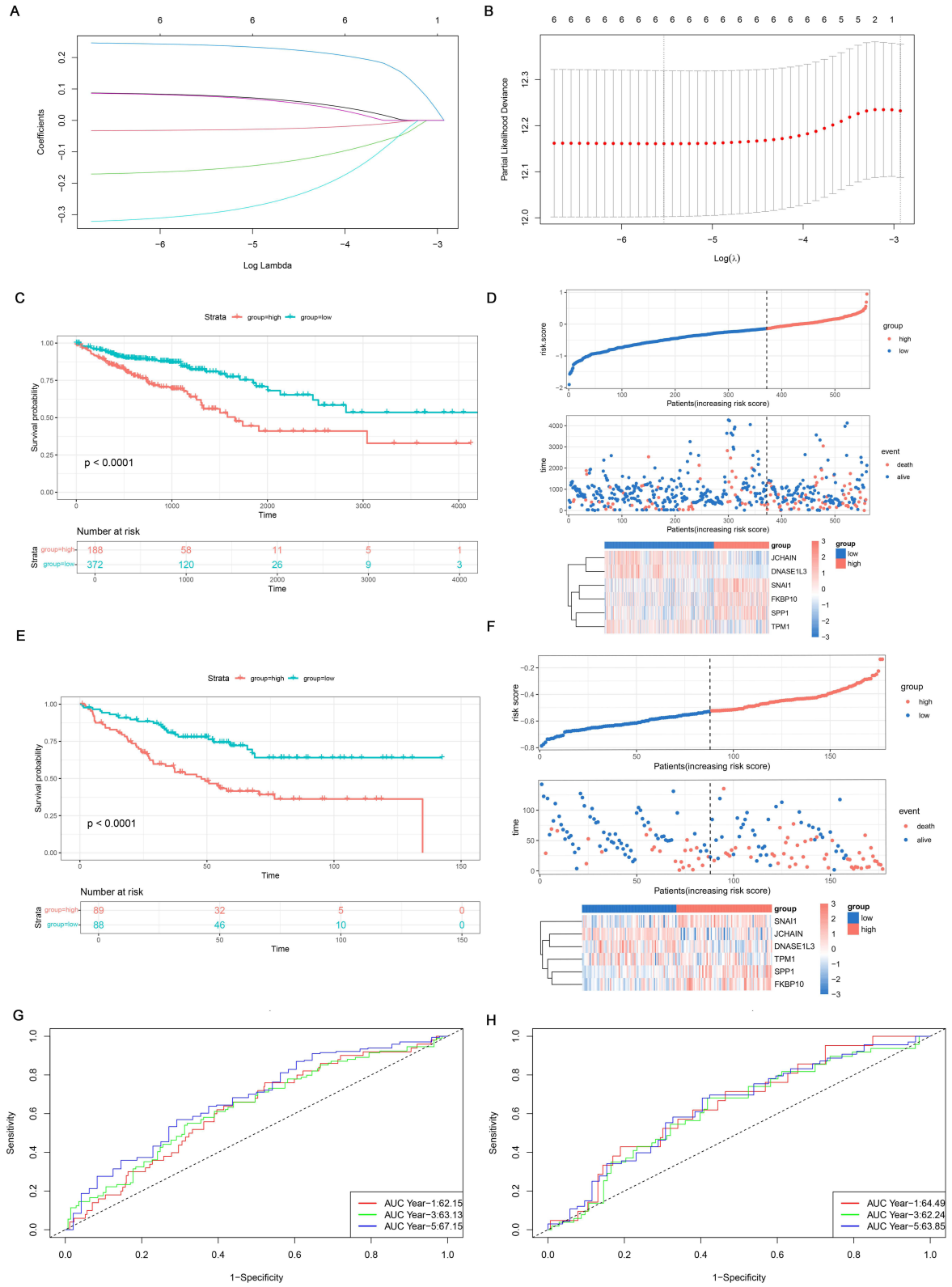

Figure 3 Construction and validation of the 6-gene prognostic risk signature. (**A** and **B**) LASSO trajectory plot of the independent variables and cross-validation curves. (**C**–**E**) Kaplan-Meier survival curves for OS in the training and validation sets. (**D** and **F**) Spatial allocation of the risk score and corresponding survival status among CRC patients in both the training and validation sets and heatmaps showing the gene expression levels of 6 key genes in high- and low-risk groups. (**G** and **H**) Time-dependent ROC curves and AUC values for 1-, 3-, and 5-year survival in training and validation sets.

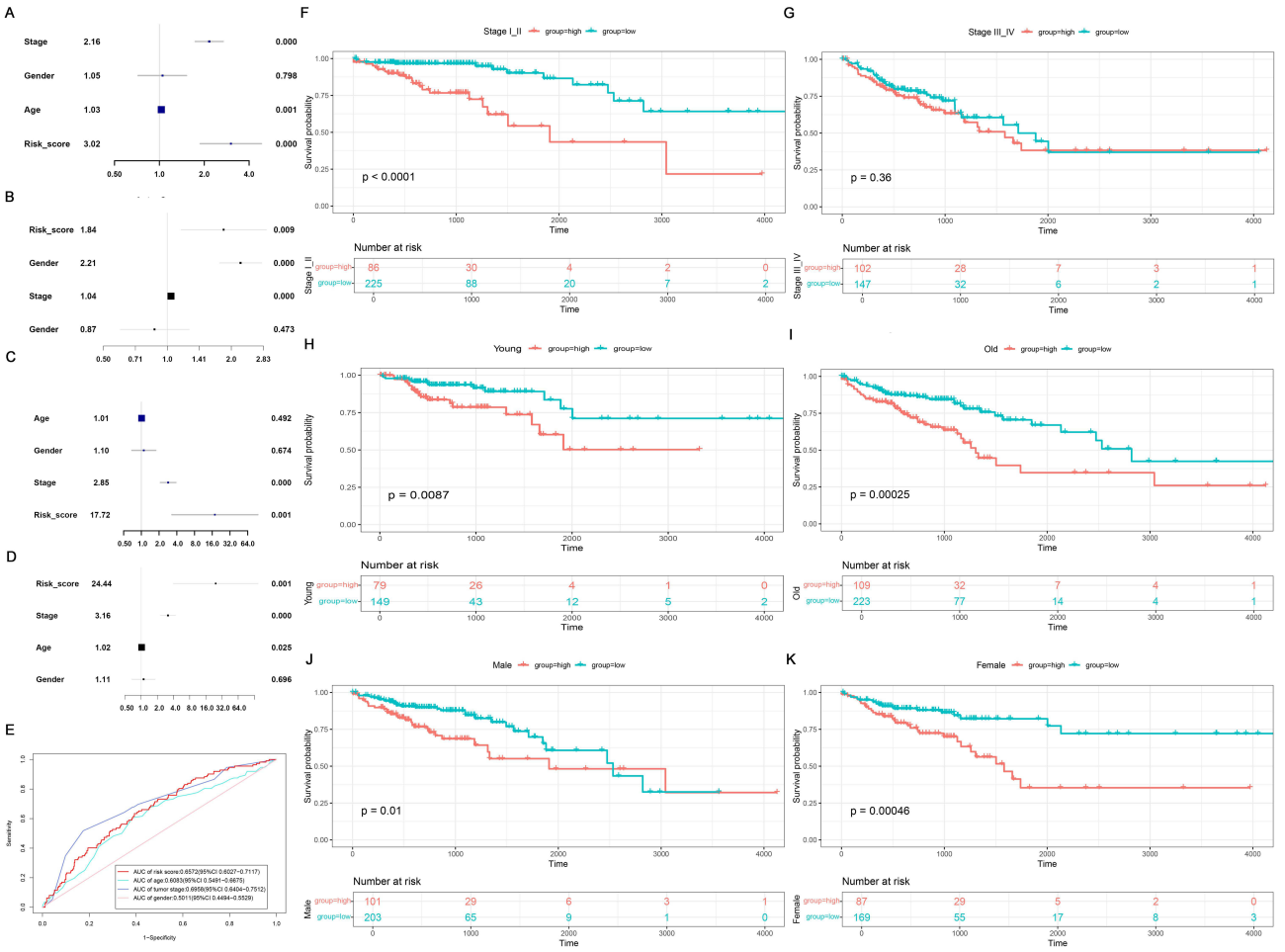

Figure 4 Associations between the risk score and clinicopathological characteristics in CRC patients. Univariate and multivariate Cox regression analyses assessing the risk score and clinicopathologic characteristics in the training (**A** and **B**) and validation sets (**C** and **D**). (**E**) The AUC values of the ROC curves comparing the risk score and clinicopathological characteristics. K-M survival analysis in CRC patients stratified by tumor stage (**F** and **G**), age (**H** and **I**) and sex (**J** and **K**).

GSE6259_CD4_TCELL_VS_CD8_TCELL_UP, GSE10325_LUPUS_CD4_TCELL_VS_LUPUS_MYELOID_DN, and GSE45365_NK_CELL_ VS_CD11B_DC_DN (Figure 6C). As evidenced by the research findings, the risk signature may be associated with the tumor immune microenvironment. How risk scores correlated with signaling pathways was evaluated using the GSVA algorithm. The results revealed a higher risk score was bound up with the majority of cancer-relevant signaling pathways, such as HIF-1, NOTCH, and HEDGEHOG signaling pathways (Figure 6D).

Somatic Variation of 6 Genes in TCGA-CRC Cohort

In our study, the somatic mutation profiles from the TCGA-CRC cohort were analyzed to identify the mutational signatures of 6 genes, and visualized between two risk groups. The data revealed relatively similar mutation profiles for all 6 genes in two risk groups. Missense mutations were the most predominant type, and single nucleotide polymorphisms (SNPs) were more frequent than deletions. Particularly, the C>T transition was the leading single nucleotide variant (SNV) type across all samples, as shown in Figure 7A and B. The mutation profiles of each of the 6 genes in CRC, and the breakdown of mutation percentages presented in Figure 7C and D. Of particular interest, APC mutations were highly prevalent among all somatic mutations in both the high- (73%, Figure 7E) and low-risk groups (75%, Figure 7F). Furthermore, our study revealed that tumors in the high-risk group exhibited a more pronounced TMB compared to those in the low-risk group, as depicted in Figure 7G. Addittionally, a notable positive correlation was observed between the risk score and TMB, as depicted in Figure 7H.

https://doi.org/10.2147/ITT.S563779

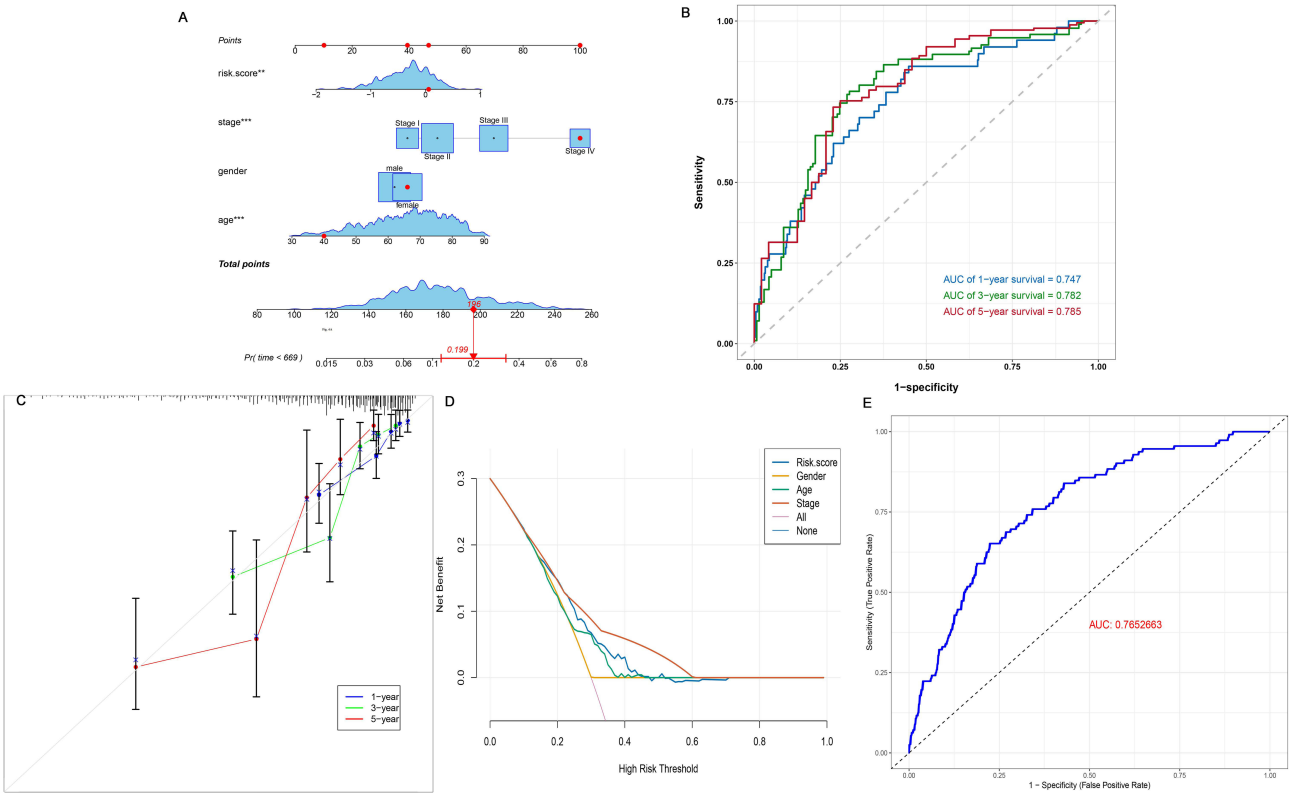

Figure 5 Construction and evaluation of the nomogram. (**A**) Nomogram for predicting OS in CRC patients. **P < 0.01, ***P < 0.001. (**B**) The ROC analysis for assessing the predictive accuracy of the nomogram. (**C**) Calibration curves evaluating the accuracy of the nomogram. (**D**) The DCA curves showing the clinical net benefit in predicting OS. (**E**) The ROC curve for the nomogram in predicting OS.

Association Between Risk Signature and Immunotherapy Response/Chemotherapy Sensitivity

Currently, immunotherapy remains ineffective for the majority of cancer patients. To clarify how the 6-gene risk score might help predict the effectiveness of immunotherapy in CRC patients, we examined the diversity in their response to immunotherapy between the two risk groups. Utilizing the TIDE database, the dysfunction, exclusion, and TIDE scores were computed for CRC patients within the TCGA-CRC cohort. We noticed that the individuals in the high-risk group exhibited elevated dysfunction, exclusion, and TIDE scores (Figure 8A–C), suggesting they were more likely to evade the monitoring of the immune system, leading to poorer immunotherapy outcomes. Furthermore, we determined that 53.9% of the patients in the low-risk group had a positive response to immunotherapy, which was strikingly higher than that in the high-risk group (Figure 8D). On top of that, we observed significant variations in the expression levels of key immune checkpoints, such as *CD274*, *HHLA2*, and *IDO2* across the high- and low-risk groups (Figure 8E). Drug sensitivity analysis indicated that patients in high-risk group exhibited reduced sensitivity to afatinib, alisertib and axitinib in comparison with those in the low-risk group (Figure 8F–H).

Exploration of Tumor Immune Infiltration Between High- and Low-Risk Groups

With an aim to explore alteration in immune infiltration, we employed the CIBERSORT and ssGSEA algorithm, providing a computational approximation of the tumor immune microenvironment. Our study revealed elevated infiltration levels of M0, M1, and M2 macrophages, along with activated mast cells, in the high-risk group. Conversely, plasma cells, resting $CD4^+$ memory T cells, and activated $CD4^+$ memory T cells exhibited reduced infiltration, as determined by the CIBERSORT algorithm (Figure 9A). Further analysis of immune infiltration and functional enrichment demonstrated a marked increase in infiltration levels of myeloid-derived suppressor cells (MDSC), natural killer (NK) cells, and

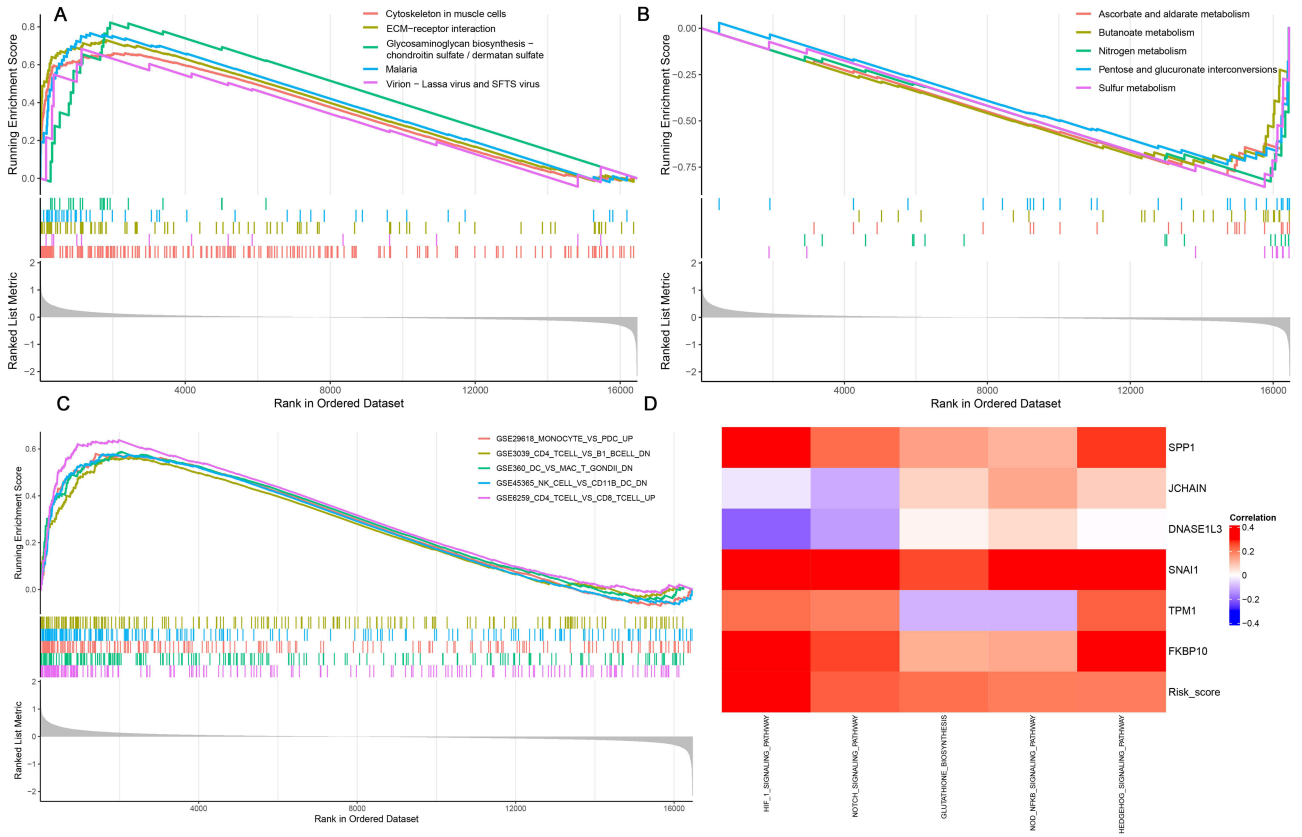

Figure 6 Functional enrichment analyses. (**A** and **B**) A marked increase in GSEA pathways across both the high- and low-risk groups. (**C**) Immune-relevant processes markedly enriched in the high-risk group. (**D**) GSVA algorithm confirmed that KEGG pathways were bound up with the risk score.

regulatory T cells (Tregs) in the high-risk group. Simultaneously, we found diminished enrichment scores for activated $CD4^+$ T cells, activated B cells, Th17 helper cells, and Th2 helper cells in the high-risk group via ssGSEA (Figure 9B).

Cell-Cell Communication Analysis Between High- and Low-Risk Groups

To investigate key cell-cell communication signaling networks, we employed the CellChat algorithm, leveraging single-cell transcriptomic data to map and quantify communication patterns. A comparative analysis was conducted between the high- and low-risk groups to identify potential alterations in cell-cell interactions associated with CRC progression. Our findings revealed enhanced intercelluar communication activity in the high-risk group, with both the frequency and intensity of interactions significantly higher (Figure 10A–C). In an effort to gain more profound insight, we focused on three key pathways (MIF, Annexin and CXCL) and examined their signaling dynamics across all cell types in both risk groups. The resulting interaction profiles were illustrated in Figure 10D–F.

Analysis of Autophagy and Metastasis Activity

The AUCell algorithm was performed to evaluate the activity score of the gene set of the autophagy and metastasis in each cell of the single-cell transcriptome. We found that both autophagy (Figure 11A) and metastasis (Figure 11B) activity scores were higher in liver metastasis tissues than in primary CRC tissues. Analysis of autophagy activity scores cell types revealed that macrophages displayed the highest autophagy activity scores across all identified cell types (Figure 11C). Likewise, examination of metastasis activity identified macrophages as one of the cell types with notably high metastasis activity scores (Figure 11D). In addition, we found that the autophagy (Figure 11E) and metastasis (Figure 11F) activity scores in the high-risk group were significantly higher than those in the low-risk group. These findings suggest that macrophages are involved in autophagy and liver metastasis of CRC, prompting us to focus subsequent analyses on their role in the CRLM microenvironment.

https://doi.org/10.2147/ITT.S563779

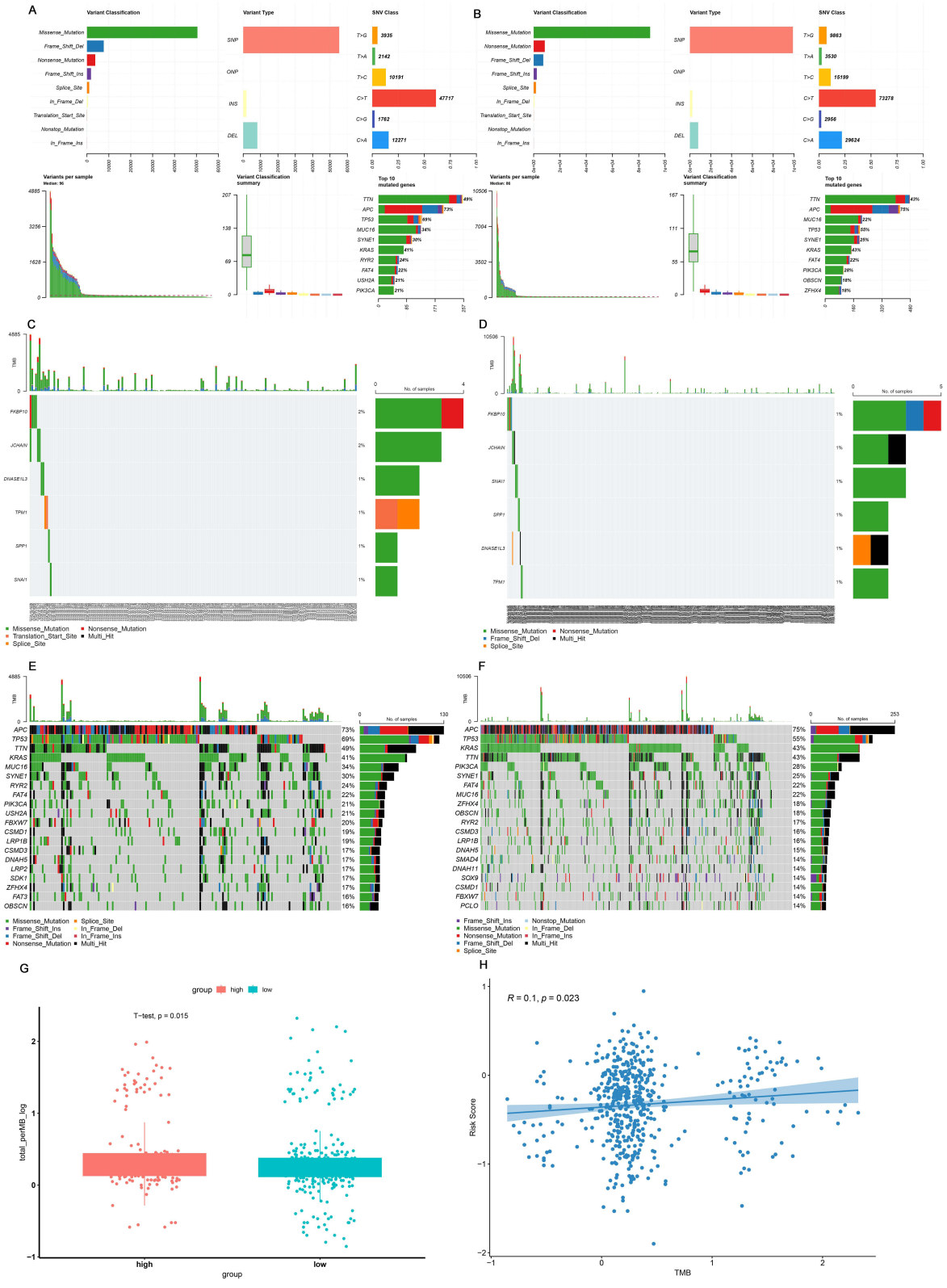

Figure 7 Analyses of tumor somatic variation and TMB correlation between high- and low-risk groups. Overview map of somatic mutations in the high- (**A**) and low-risk (**B**) groups. Somatic mutation characteristics of 6 genes in the high- (**C**) and low-risk (**D**) groups. Gene mutation accumulation in high- (**E**) and low-risk (**F**) groups. TMB comparison between groups (G) and correlation analysis between risk score and TMB (H).

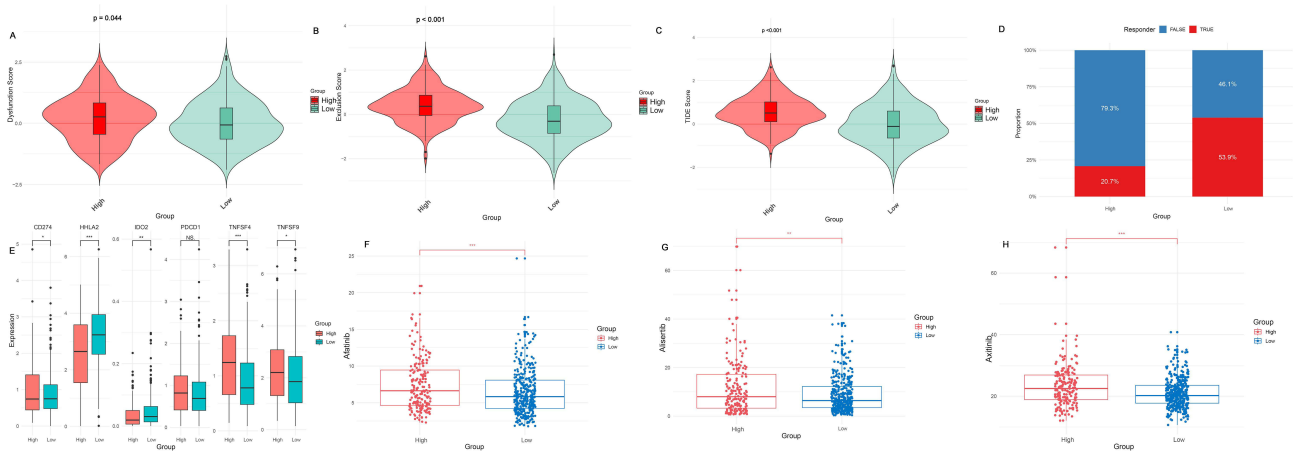

Figure 8 Prediction of response to immunotherapy and drug sensitivity. (**A**–**D**) Comparison of TIDE prediction scores across these two risk groups. (**E**) Expression levels of three key immune checkpoint genes between between high- and low-risk groups. *P < 0.05, **P < 0.01, ***P < 0.001; ns, not significant. (**F**–**H**) Assessment of sensitivity to anti-cancer drugs (afatinib, alisertib and axitinib) between these two risk groups. **P < 0.01, ***P < 0.001.

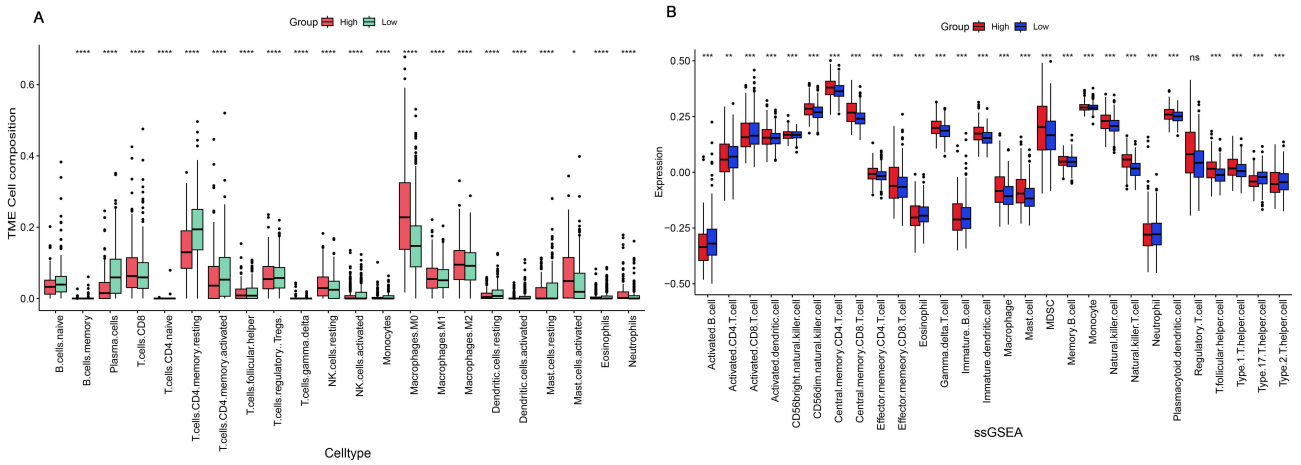

Figure 9 Exploration of immune cell infiltration between two risk groups. Boxplots of all immune responses across these two risk groups based on the CIBERSORT (**A**) and ssGSEA (**B**) algorithms. *P < 0.05, **P < 0.01, ***P < 0.001,****P < 0.0001; ns, not significant.

Characterization of Macrophages Heterogeneity and Dynamics

To gain deeper insight into the functional role of macrophages, six macrophage subpopulations were identified via re-clustering, as shown in Figure 12A. Canonical macrophage markers were used to confirm the identity of these subpopulations (Figure 12B). A pseudotemporal trajectory to trace cell differentiation was then established, which revealed that the pseudotime increased from *TNF*$^{+}$ macrophage and *CXCL9*$^{+}$ macrophage to *MRC1*$^{+}$ macrophage and *SPP1*$^{+}$ macrophage (Figure 12C and D). Along this trajectory, both autophagy and metastasis activity scores showed a progressive increase (Figure 12E). Expression of canonical M1 macrophage markers (*TNF* and *CXCL9*) decreased, whereas the expression of the M2 marker *MRC1* increased. Notably, the expression trend of *SPP1* aligned with that of *MRC1*, increasing over pseudotime, which further supports its role as a pro-tumorigenic gene within the M2-like macrophage population during CRLM progression (Figure 12F). Taken together, these findings suggest that *SPP1* not merely a marker but a functional orchestrator in tumor-associated macrophages. Its expression couples heightened autophagic activity with pro-metastatic potential, identifying it as a key driver of the immunosuppressive and metastasis-prone niche in CRC.

https://doi.org/10.2147/ITT.S563779

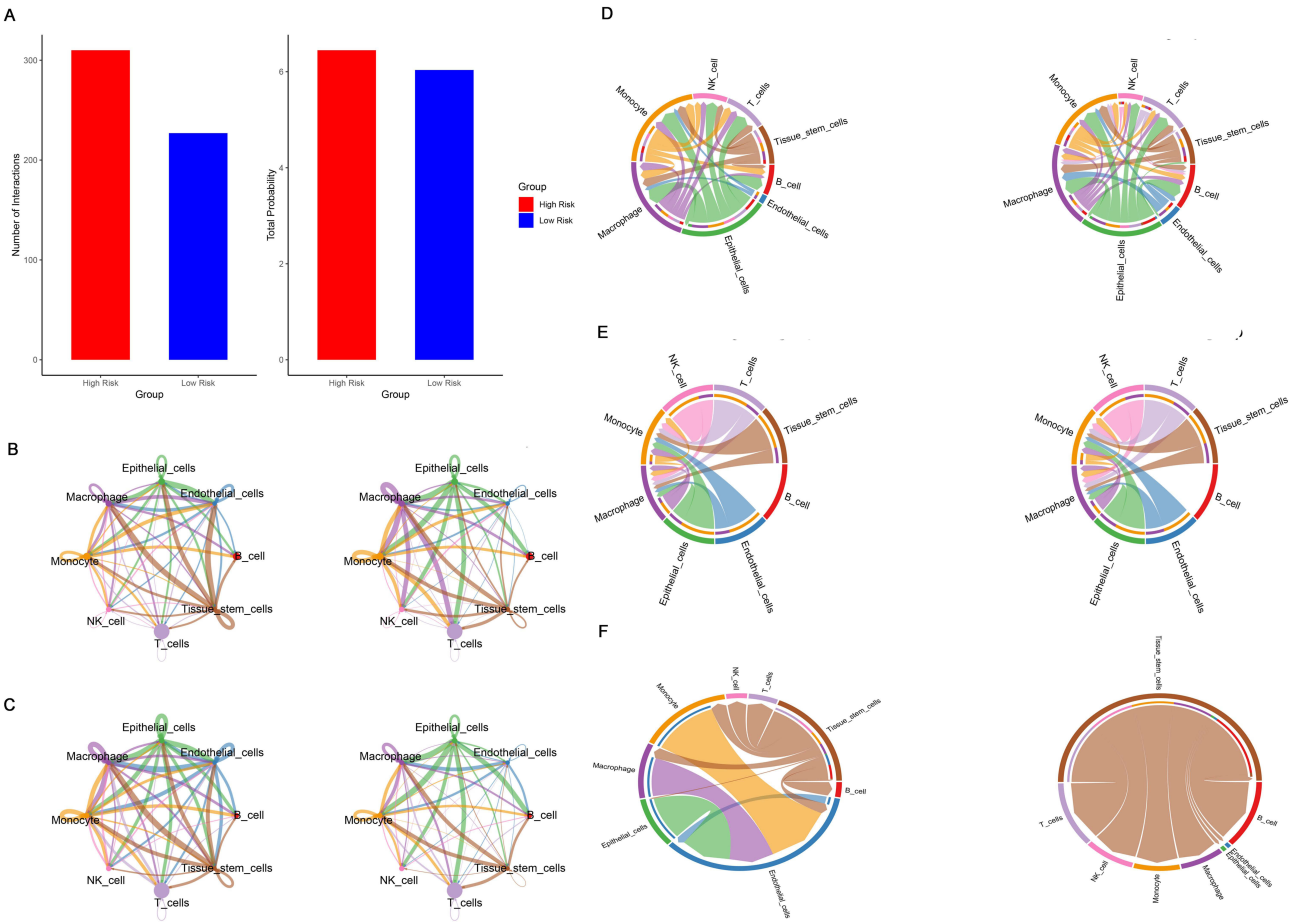

Figure 10 Cell-cell communication analysis between these two distinct groups. (**A**) The number and strength of intercellular interactions between the high- and low-risk groups. Circle plots of number and strength between immune cells and tumor cells in high- (**B**) and low-risk group (**C**) for cell-cell communication. MIF signal pathway (**D**), Annexin signal pathway (**E**) and CXCL signal pathway (**F**) in high- and low-risk groups.

Expansion and Functional Characterization of an Exhausted CD8$^+$ T Cells

Cell clustering was performed to explore the heterogeneity of *CD8*$^+$ T cells. The *CD8*$^+$ T cells were classified into distinct subtypes, including exhausted *CD8*$^+$ T cells, effector *CD8*$^+$ T cells and memory *CD8*$^+$ T cells (Figure 13A). The canonical *CD8*$^+$ T cell markers were used to further validate (Figure 13B). The results showed that the proportion of exhausted *CD8*$^+$ T cells was the highest in both liver metastasis tissues (Figure 13C) and high risk group (Figure 13D). A pseudotemporal trajectory to trace cell differentiation was then established, which revealed that the pseudotime increased from effector *CD8*$^+$ T cells and memory *CD8*$^+$ T cells to exhausted *CD8*$^+$ T cells (Figure 13E and F). Across subsets, exhausted *CD8*$^+$ T cells exhibited the highest autophagy and metastasis activity scores (Figure 13G). Moreover, we explored the trend of *SPP1* and immunosuppressive checkpoint gene expression, including cytotoxic T lymphocyte antigen 4 (*CTLA-4*), hepatitis A virus cellular receptor 2 (*HAVCR2*), lymphocyte activating 3 (*LAG3*), programmed cell death 1 (*PDCD1*) and T cell immunoreceptor with Ig and ITIM domains (*TIGIT*) over pseudotime and found that their expression increased gradually (Figure 13H). Furthermore, the highest percentage of *SPP1*-positive cells (expression > 0) was found in exhausted *CD8*$^+$ T cells (Figure 13I), which suggesting the link between exhaustion, *SPP1* expression, and poor prognosis. Consequently, *SPP1* emerges with a dual role in immune evasion: beyond its functions in macrophages, it is specifically enriched within exhausted *CD8*$^+$ T cells, suggesting its active involvement in perpetuating T cell dysfunction and facilitating an immune-tolerant microenvironment favorable for metastatic outgrowth.

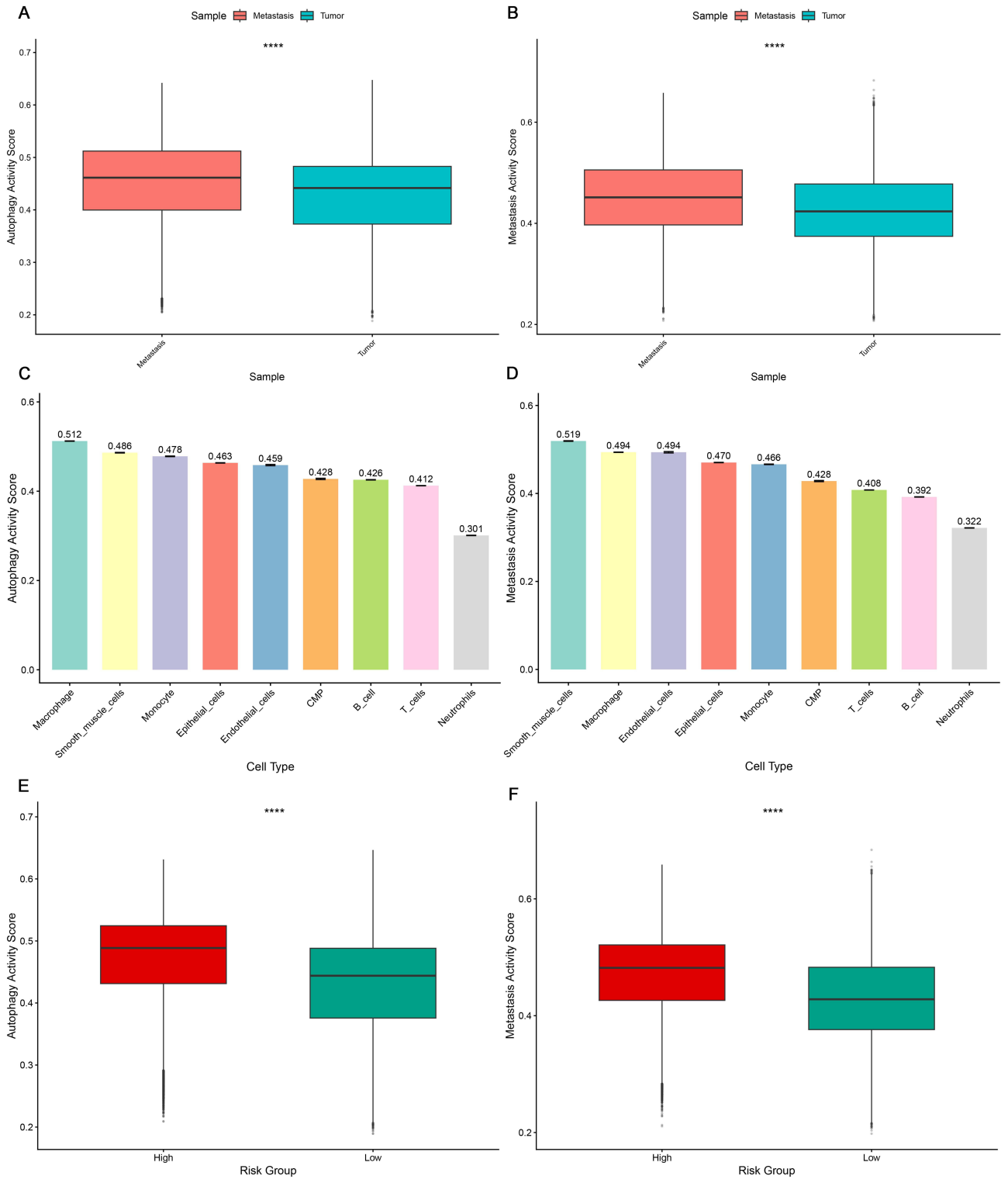

Figure 11 Autophagy and metastasis activity scores between liver metastasis and primary tumor. The comparison of autophagy (**A**) and metastasis (**B**) activity scores between primary CRC tumors and liver metastasis tissues. ***P < 0.001. Comparison of autophagy (**C**) and metastasis (**D**) activity scores across different cell types. Comparison of autophagy (**E**) and metastasis (**F**) activity scores between high- and low-risk groups. ***P < 0.001.

https://doi.org/10.2147/ITT.S563779

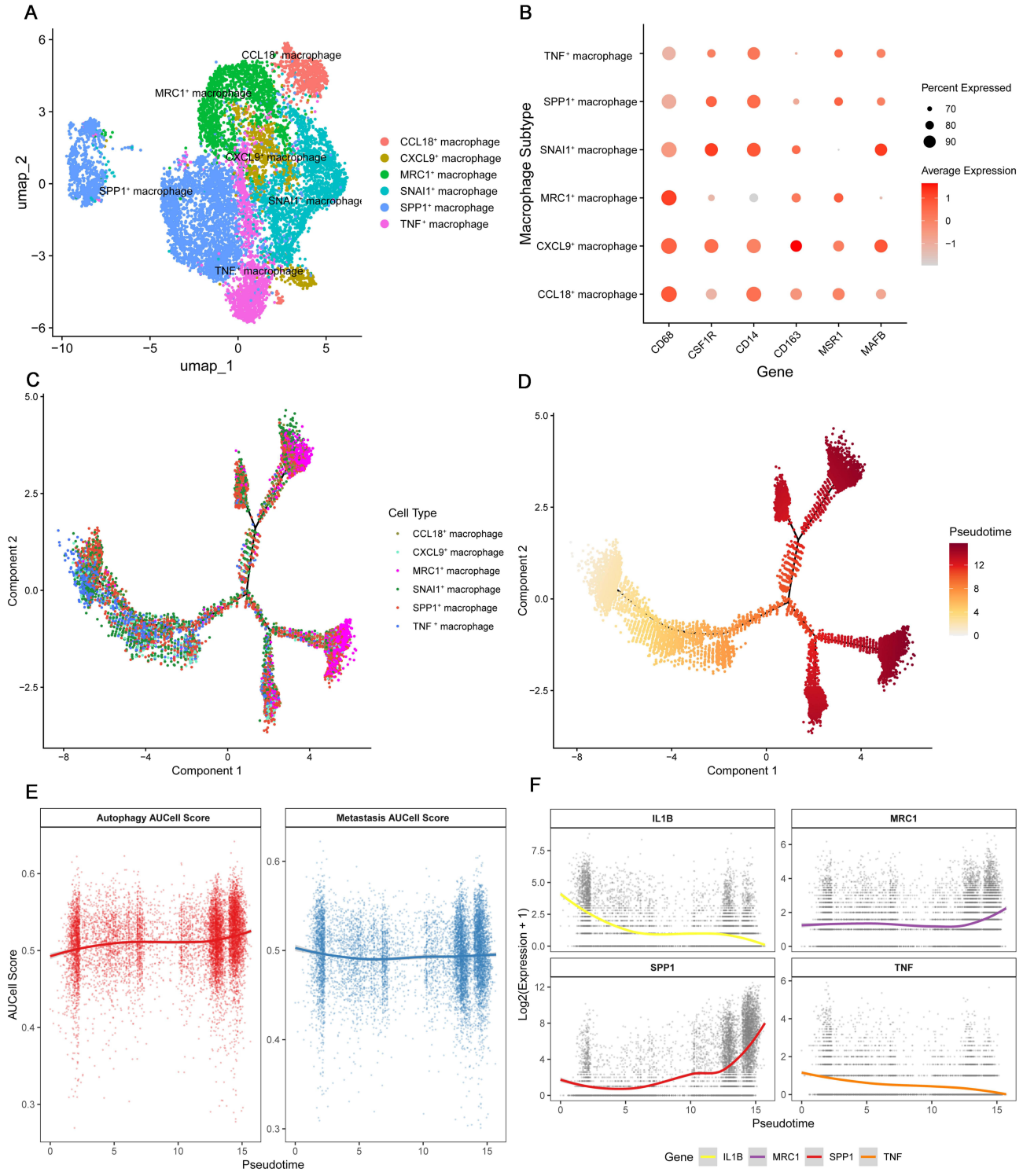

Figure 12 Subpopulation characterization and trajectory analysis of macrophages (**A**) Classification and annotation of macrophages. (**B**) Dot plot illustrating the expression levels of canonical macrophage marker genes across the identified subpopulations. (**C** and **D**) The results of pseudotime analysis in different macrophage s. (**E**) Dynamics of autophagy and metastasis activity scores along the pseudotime trajectory. (**F**) Gene expression dynamics of key markers (*SPP1*, *IL1B*, *MRC1*, *TNF*) along the pseudotime trajectory. Lines represent the smoothed expression trend (loess regression) for each gene, illustrating their coordinated or divergent regulation during macrophage state transitions.

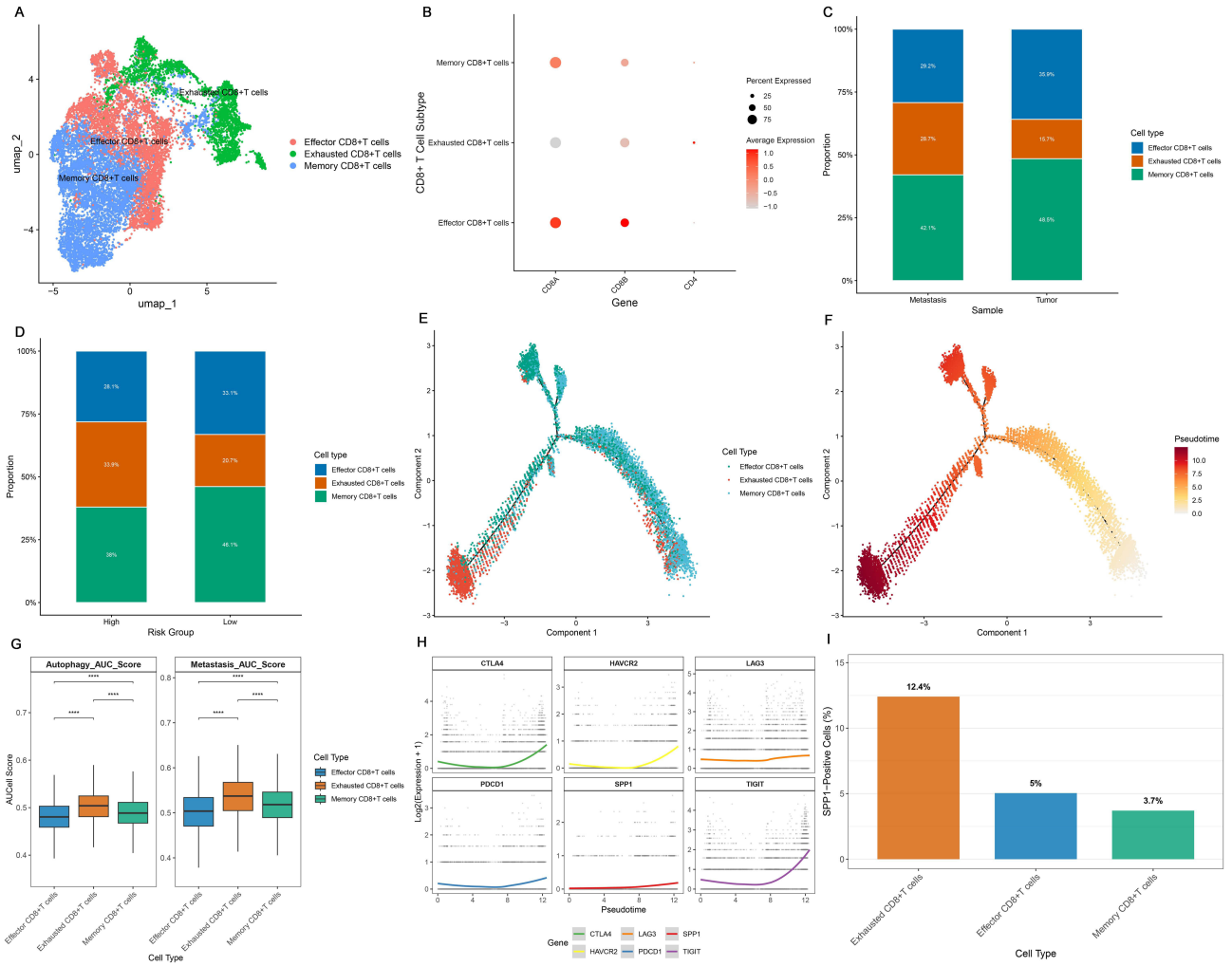

Figure 13 Heterogeneity, distribution, and dynamics of *CD8*$^+$ T cells (**A**) Annotations for *CD8*$^+$ T-cell subtypes. (**B**) Dot plot validating the identity of *CD8*$^+$ T cell subtypes by displaying the expression of canonical *CD8*$^+$ T cell markers. The proportion of *CD8*$^+$ T-cell subtypes in different tissues (**C**) and risk groups (**D**). (**E** and **F**) The results of pseudotime analysis in different *CD8*$^+$ T-cell subtypes. (**G**) Box plots comparing the autophagy and metastasis activity scores across different *CD8*$^+$ T cell subsets. ***P < 0.001. (**H**) Dynamic expression patterns of *SPP1* and immunosuppressive gene expression (*CTLA4*, *HAVCR2*, *LAG3*, *PDCD1* and *TIGIT*). (**I**) Bar plot displaying the percentage of *SPP1*-positive cells within each *CD8*$^+$ T cell subset.

Co-Expression Network Analysis of the Six Signature Genes

The co-expression network revealed distinct interaction patterns among the six key genes (Figure 14A). *SPP1*, *SNAI1*, and *FKBP10* formed a tightly interconnected triangle, indicating strong coordination among these risk-associated genes. Meanwhile, *DNASE1L3* and *TPM1* showed association with *SPP1*, suggesting more complex regulatory relationships within the gene set. Taken together, the results highlighted the central role of *SPP1* within the six key genes. To elucidate the potential cooperative roles of the six key genes, we performed GSVA. The results suggested *SPP1* may promote tumor progression by MAPK, JAK-STAT, and KRAS signaling pathways, and interacting with the immune microenvironment through T cell exhaustion- and macrophage polarization-mediated mechanisms (Figure 14B).

Validation of the Expression and Prognostic Value of Autophagy and Liver Metastasis Related Hub Genes

In our study, a prognostic risk signature, which consisted of 6 genes, was identified. To further confirm the predictive power of the risk signature, experimental validations were conducted to determine the expression levels and prognostic significance of the 3 risk genes. Our results demonstrated that *SPP1* was primarily expressed in monocytes and

https://doi.org/10.2147/ITT.S563779

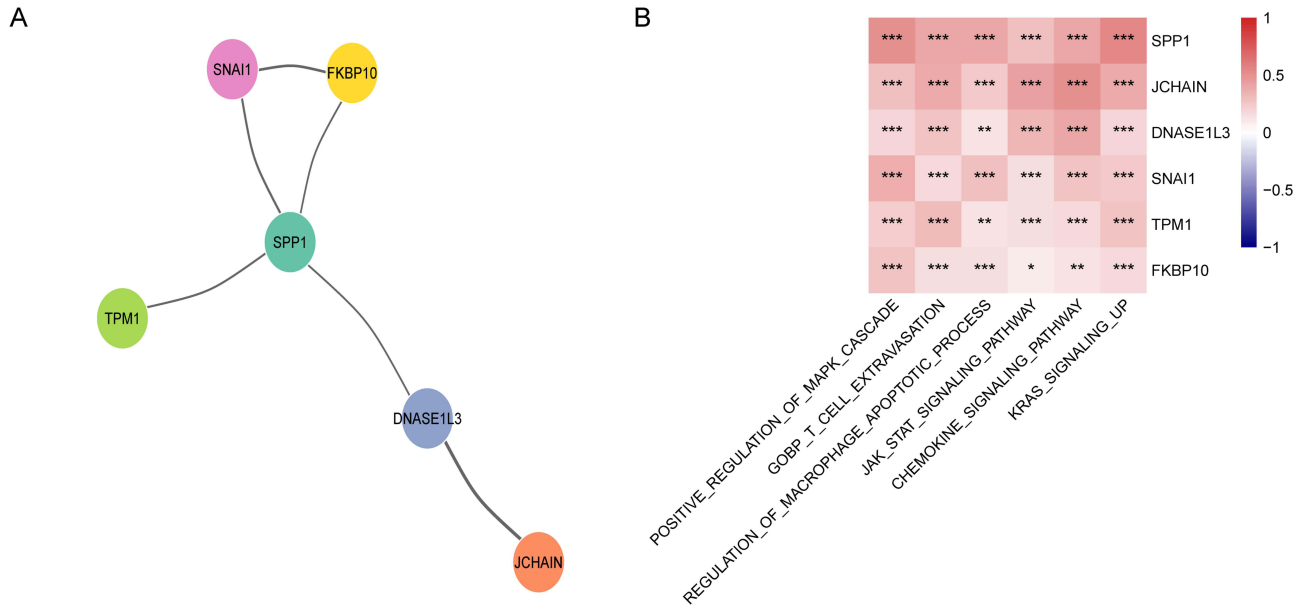

Figure 14 The relationship and reveals pathway associated with risk signature gene (**A**) The co-expression network among six key risk signature genes. (**B**) Correlation heatmap of six key signature genes with selected pathways from GSVA analysis. *P < 0.05, **P < 0.01, ***P < 0.001.

macrophages, *JCHAIN* predominantly expressed in B cells, *SNAI1* mainly expressed in endothelial cells, *TPM1* and *FKBP10* primarily expressed in tissue stem cells, and *DNASE1L3* showed relatively low expression levels across different cell populations (Figure 15A, Supplementary Figure 4). Further analysis indicated that *SPP1*, *SNAI1*, and *FKBP10* were independent prognostic risk factors for CRC, which may be tightly correlated with the progression and metastasis of CRC. Therefore, we delved further into the expressions of *SPP1*, *SNAI1*, and *FKBP10* between adjacent tissues and tumor tissues. Elevated protein levels of *SPP1*, *SNAI1*, and *FKBP10* were detected in tumor tissues (Figure 15B, Supplementary Figure 6). IHC staining results showed that the expressions of *SPP1*, *SNAI1*, and *FKBP10* in liver metastatic tissues were significantly higher than those in primary CRC tumor tissues and adjacent normal tissues (Figure 15C).

Discussion

Notwithstanding remarkable breakthroughs in surgery, chemotherapy, and targeted or immune checkpoint inhibitors therapies for CRC over the past few decades, the 5-year survival rate was still a major concern. Moreover, treatment failures were linked to the spread and metastasis of cancer.[26,27] The liver was the primary organ targeted by CRC metastasis. Roughly 25% of CRC patients were diagnosed with synchronous liver metastasis, while 50% developed metachronous liver metastasis within 3 years subsequent to initial treatments.[28] It was particularly noteworthy that recent research has underscored the paramount significance of autophagy in tumor metastasis. The spread and invasion of highly metastatic cells were facilitated by autophagy,[29,30] potentially through mechanisms involving focal adhesions.[31,32] Numerous biomarkers associated with CRC liver metastasis have been identified, such as certain protein-coding genes and long non-coding RNA.[33,34] Prognostic risk models of liver metastasis or autophagy-related genes alone had demonstrated striking clinical predictive power.[35–38] Due to the dual effect of autophagy, the gene transcription and translation of a single autophagy-related gene has limited ability to evaluate the cancer status and prognosis, while the gene transcription and translation of liver metastasis-related genes proved that the cancer was in the advanced stage and invasive. The combination of the autophagy- and liver metastasis-related genes may have more significant value for the prognosis of CRC patients. Nonetheless, current research had effectively combined the significant roles of autophagy and liver metastasis in CRC. It remains imperative to establish a prognostic risk model that accounts for the synergistic impact of both factors, which would offer invaluable guidance to clinicians for assessing patient prognosis and tailoring individualized treatment plans.

In this study, we established an innovative prognostic risk signature for CRC patients, utilizing a combination of 6 genes linked to autophagy and liver metastasis. We established and verified the prognostic risk signature in the TCGA and GEO databases. Both univariate and multivariate Cox regression analyses confirmed the risk score as an independent predictor of CRC patients. Furthermore, GSEA pinpointed increased activity of cancer-related pathways among high-risk patients, with these pathways closely tied to the risk score. The predictive nomogram suggested exceptional precision in

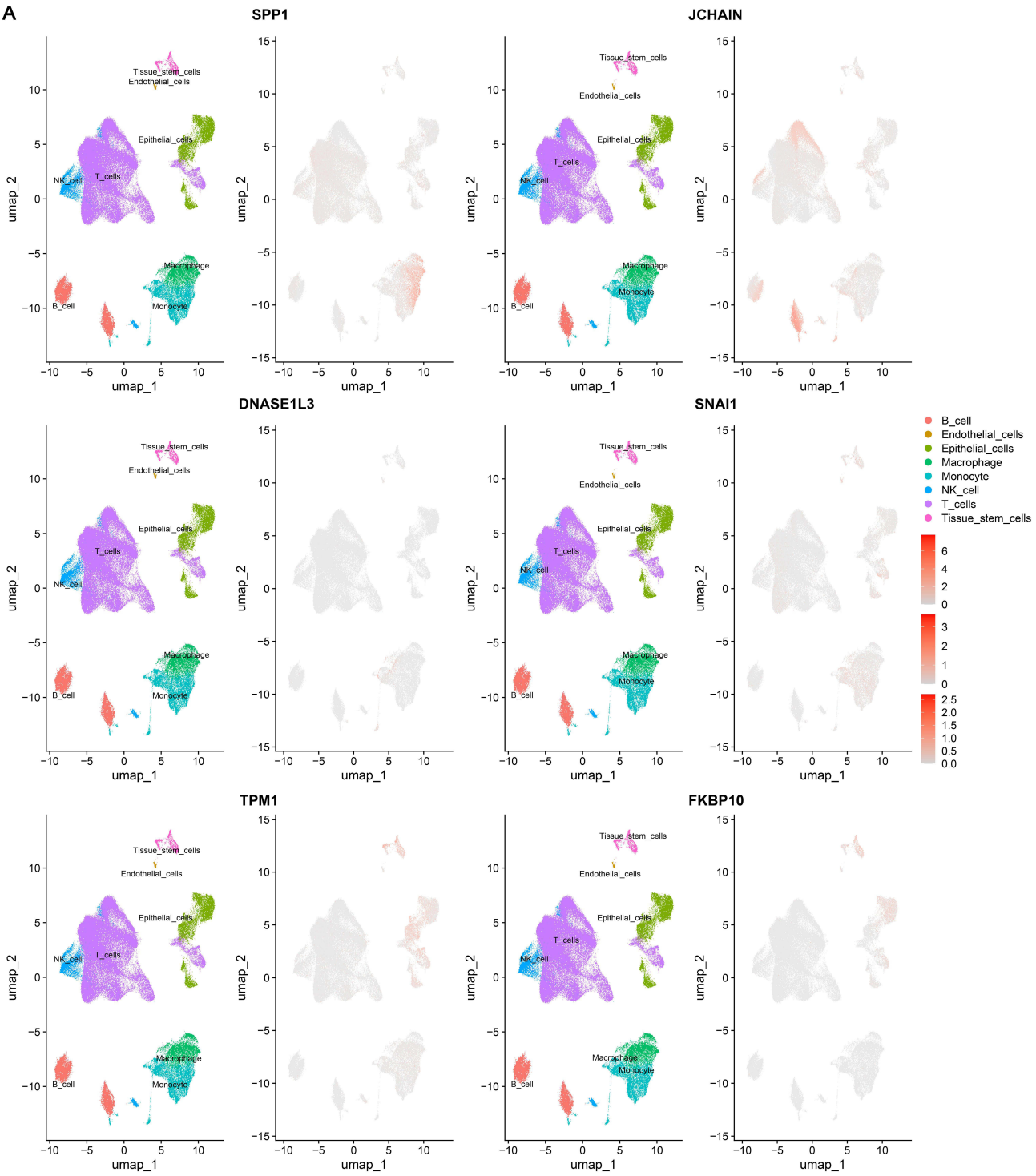

Figure 15 Continue.

https://doi.org/10.2147/ITT.S563779

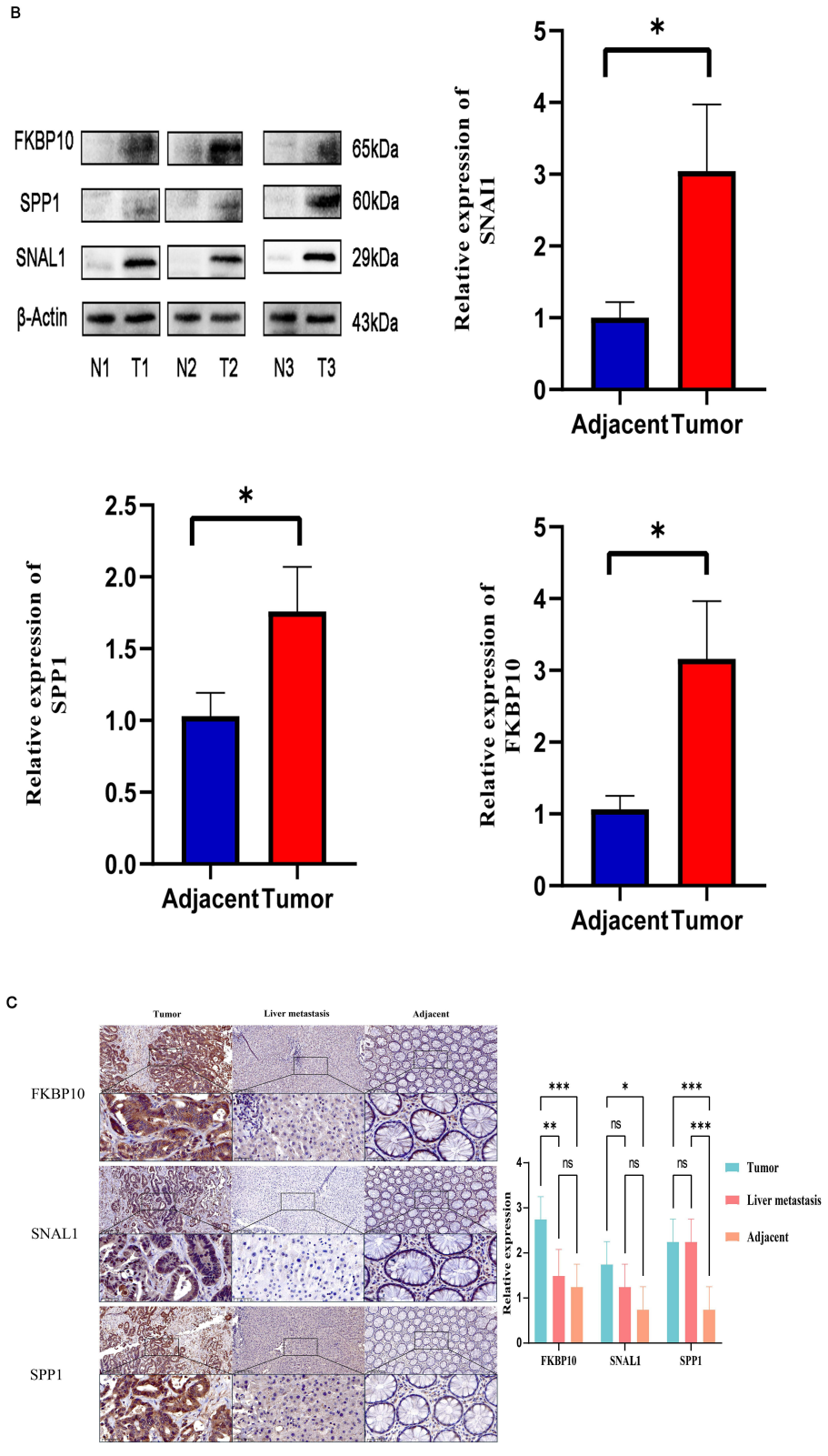

Figure 15 Identification of the expression levels of 3 risk genes and prognosis of 6 genes (**A**) The distribution of genes in different cell types in single-cell dataset. (**B**) Protein expression levels of *SPP1*, *SNAI1*, and *FKBP10* in adjacent tissues and CRC tissues assessed by WB. *P < 0.05. (**C**) Representative images from IHC staining of *SPP1*, *SNAI1*, and *FKBP10* in adjacent tissues, primary CRC tumor tissues and liver metastasis tissues. *P < 0.05, **P < 0.01, ***P < 0.001.; ns, not significant.

https://doi.org/10.2147/ITT.S563779

estimating survival probabilities at 1, 3, and 5 years. Drug sensitivity analysis also highlighted stark disparities in treatment responses across risk groups, which could be invaluable in determining the best course of adjuvant chemotherapy or targeted therapy for non-resectable or post-operative CRC patients. From a clinical perspective, incorporation of this risk score into existing clinical workflows could help clinicians identify patients at high risk of disease progression or liver metastasis who may benefit from intensified surveillance, closer follow-up, or earlier systemic intervention, while sparing low-risk patients from unnecessary overtreatment. In this context, the proposed signature has the potential to complement conventional clinicopathological parameters and support more personalized treatment planning for CRC patients.

We identified 6 genes: *SPP1*, *JCHAIN*, *DNASE1L3*, *SNAI1*, *TPM1* and *FKBP10* as potential prognostic markers (Supplementary Figure 5A–F). *JCHAIN*, *DNASE1L3*, and *TPM1* were found to be protective factors, while *SPP1*, *SNAI1*, and *FKBP10* were appeared to be risk factors. *SPP1*, an immunological marker related to CRLM,[39] was correlated with less favorable survival outcomes.[40] A research by Zheng et al suggested that knocking down *SPP1* could suppress SW620 cell proliferation and migration, possibly through its interaction with M2 macrophage-mediated pro-tumor effects.[38] Expanding on this, Liu et al put forth a standpoint that $SPP1^{+}$ macrophage subtypes accelerated CRC liver metastasis by reinforcing tumor cell invasion.[41] Mechanistically, tumor-derived extracellular vesicles enriched with circ-0034880 facilitate communication between CRC cells and $SPP1^{high}CD206^{+}$ pro-tumor macrophages, thereby pushing ahead pre-metastatic niche formation and CRLM. In particular, ginsenoside *Rb1* has emerged as a potential therapy to suppress this process and prevent CRLM.[42] Other than CRC, *SPP1* has been implicated in autophagy regulation in prostate[43] and hepatocellular cancers.[44] As the main transcriptional repressor of *E-cadherin*,[45] *SNAI1* emerges as a paramount player in EMT, which is a critical process in development of various cancers. Dysregulation of *SNAI1* could trigger EMT.[46] A study illustrated that *MACC1* accelerated EMT by boosting transcriptional activity of *SNAI1*, transactivating *FN1* and repressing *CDH1*, thereby encouraging pancreatic cancer liver metastasis.[47] Apart from that, over-expressing circRNALIFR-007 could suppress *SREBF1* and *SNAI1*, thus suppressing breast cancer liver metastasis.[48] The role of autophagy in EMT, nevertheless, remained a hotly debated topic. On the one hand, autophagy could degrade the *SNAI1* protein, stifling autophagy may in turn stimulate EMT.[49,50] On the other hand, autophagy had also been shown to promote EMT by degrading *E-cadherin* or up-regulated *TGF-β1* expression.[51,52] *FKBP10* belongs to a family of immunophilins characterized by repeating peptidylprolyl isomerase domains.[53] Chen et al had shown that the *circREEP3-FKBP10* axis was a driving force in the progression and metastasis of CRC.[54] Additional research demonstrated a more tight correlation between *FKBP10* and autophagy in renal cancer[55] and bladder cancer,[56] as well as with EMT in gastric cancer.[57] *DNASE1L3*, generally included to be down-regulated in CRC,[58] inhibited on tumor cell proliferation and migration.[59] Further research by Li et al suggested its role in enhancing anti-tumor immunity and expediting the progression of colon cancer in murine.[60] As an extensively acknowledged tumor suppressor, *TPM1* was typically down-regulated in CRC.[61] Evidence suggested that *MYC*-induced *ELFN1-AS1* recruited *EZH2* and *FOXP1* to suppress *TPM1*, enhancing CRC progression.[62] Likewise, *LINC01116* inactivated the *TPM1* promoter through *EZH2*, driving CRC proliferation and angiogenesis.[63]

Our study identified *SPP1* not merely as a marker distinguishing macrophage subpopulations, but as a central functional executor and coordinator of tumor-promoting immune programs. *SPP1* served as a diagnostic and prognostic marker for CRC, and its blockade could suppress tumor progression and metastasis.[38,64] Further studies indicated that $SPP1^{+}$ macrophages were closely associated with malignancy and liver metastasis in CRC.[41] Our study revealed that autophagy- and metastasis-related programs were enriched in $SPP1^{+}$ macrophages, suggesting that autophagy may provide the key metabolic foundation supporting their pro-metastatic function. This demonstrated that *SPP1* played a crucial role in driving macrophages toward a dual-polarization state characterized by both "metabolic reprogramming" and "pro-metastatic" activities. Therapeutically, Zhou et al showed that tetrahydrocurcumin inhibited M2-like macrophage polarization via the *SPP1/CD44* axis, thereby modulating the tumor immune microenvironment and exerting anti-tumor effects.[65] Xie et al further demonstrated that preoperative chemotherapy significantly reduced *SPP1* expression in macrophages, especially in treatment responders.[66] Together, these results supported the feasibility of targeting $SPP1^{+}$ macrophages for therapeutic intervention. In the tumor microenvironment, exhausted T cells that arise due to chronic antigen exposure exhibit a gradual loss of effector function, continuously express multiple inhibitory receptors such as

PDCD1 and *CTLA-4*, and show impaired proliferative potential.[67] Our research has found that *SPP1* may be actively involved in the establishment and maintenance of T-cell functional exhaustion. This discovery elevated *SPP1* from a traditional tumor-promoting factor to a key regulatory factor linking immune suppression and immune escape. Furthermore, exhausted T cells played a key role in immunotherapy. Immune checkpoint inhibitors, including anti-PD1 and anti-CTLA-4 therapies, had been shown to reverse T-cell exhaustion and bring about durable clinical responses in some patients.[68–71] A study indicated that exhausted T cells could promote the process of CRLM, thereby facilitating tumor formation.[72] This provided a new perspective for the treatment and diagnosis of CRC. Therefore, therapeutic strategies targeting *SPP1* may not only hinder the formation of a pro-metastatic immune microenvironment but also directly alleviate T cell exhaustion, thereby releasing endogenous anti-tumor immunity. Collectively, our results defined *SPP1* as a central immunoregulatory node integrating metabolic adaptation, macrophage-driven metastasis, and adaptive immune dysfunction. This integrated immunometabolic feature indicated that patients in high-risk group may be particularly suitable for receiving treatment strategies targeting the immune tumor microenvironment centered on *SPP1*, including interventions such as reprogramming of macrophages, metabolic regulation, or reversal of T cell exhaustion.

The exploration of the tumor immune infiltration in CRC revealed key immune responses.[73] We observed elevated levels of immature B cells, immature $CD4^+$ T cells, activated memory $CD4^+$ T cells, neutrophils, and T cells in the low-risk group. The immature B cells acted as the forerunners of active B cells, which correlated with higher survival rates, especially in high-grade tumors, where certain B cell markers could extend lifespan.[74] T cells and neutrophils play a key role in destroying tumor cells and providing robust anti-tumor defenses. For this reason, patients in the low-risk group were inclined to yield more favorable survival outcomes.[75] In contrast, the high-risk subgroup revealed proportions of M0/M1/M2 macrophages and MDSCs, which aligns with previous findings.[76,77] Regulatory T cells engaged with M2 macrophages, dampening the anti-tumor responses of CRC and M0 macrophages, which exhibit tumor-promoting properties.[78] As evidenced by relevant studies, M2 macrophages suppressed the functions of Th1, Th2 and $CD4^+$ T cells, cytotoxic T lymphocytes, and NK cells through the secretion of anti-inflammatory cytokines.[79,80] This suppression may compromise the ability of immune system to detect and combat tumor cells, thereby fostering an immune evasion microenvironment that encouraged tumor cell growth and invasion. Moreover, M2 macrophages potentially give rise to angiogenic factors like *VEGF*,[81] accelerating the development of new blood vessels and facilitating the spread of tumor cells, thereby expediting CRC progression. On top of that, MDSCs not only inhibited the activities of effector immune cells but also drove tumor angiogenesis and metastasis.[82,83] These findings suggested that the high-risk subgroup was at a more remarkable risk of immune suppression than the low-risk subgroup.[84] Lower TIDE scores in the low-risk group suggested more dramatic sensitivity to immunotherapy treatments.Conversely, high-risk patients exhibited activation of JAK-STAT, MAPK, PI3K-Akt, Rap1 and Wnt signaling pathways, underlining potential avenues for therapeutic intervention.

By further exploring the cell-cell communication between the high- and low-risk groups uncovered some fascinating insights. Specifically, the MIF, CXCL, and Annexin signaling pathways stood out as uniquely active in the high-risk group. The MIF receptor consists of a ligand-locked *CD74* complex and a signaling-linked *CD44*. Once ligands latch onto MIF, it could initiate downstream signal transduction to promote inflammation and cell survival.[85] CXCL is like a magnet for white blood cells, leading them to the site of inflammation. They bind to the corresponding CXC chemokine receptor to trigger the internalization and transduction of downstream signal transduction pathways.[86] The influence of CXCL on tumor growth and metastasis was undeniable.[87–89] The Annexin family has been a hot topic in CRC research, acting as biomarkers with a direct link to tumor progression and metastasis. Notable players include *Annexin A5*,[90] *Annexin A2*[91] and *Annexin A9*.[92]

Limitations

This study has several limitations. Firstly, we relied heavily on publicly available datasets, which may affect model generalizability. Secondly, while our findings strongly support an immunometabolic link between autophagy-associated programs and liver metastasis, we acknowledge that causal validation will require dedicated functional studies. Future work will prioritize experimental validation. Thirdly, the sample size in our experimental validation phase remains relatively limited. Future studies with larger, independent cohorts are needed to substantiate these initial findings. Fourthly, we still need to dig deeper into the biological roles of the autophagy genes we found out through cell and

animal experiments and how they actually contribute to CRLM on a mechanistic level. Finally, while differences between risk subgroups were characterized, identifying synergistic therapeutic strategies for these groups remains critical.

Conclusions

In conclusion, we developed a novel prognostic risk signature comprising six autophagy- and liver metastasis-related genes (*SPP1*, *JCHAIN*, *DNASE1L3*, *SNAI1*, *TPM1* and *FKBP10*) to explore and elucidate the liver metastasis and autophagy on prognosis of CRC patients. Our study proposed a novel immunometabolic nexus model for CRLM, uncovering the synergistic crosstalk between autophagic adaptation and pro-metastatic signaling. We identified *SPP1* as a functional hub that couples pro-metastatic signaling with autophagic adaptation, specifically within macrophages and exhausted $CD8^+$ T cells. Therapeutically, this re-framed $SPP1^+$ immune cells not merely as biomarkers but as potential therapeutic targets for disrupting the functional synergy that enables liver metastasis. Collectively, our work provides a promising prognostic tool and therapeutic direction for personalized management of CRC.

Abbreviations

CRC, Colorectal cancer; WGCNA, Weighted gene co-expression network analysis; CRLM, Colorectal liver metastases; EMT, Epithelial-mesenchymal transition; FPKM, Fragments per kilobase per million mapped reads; ARGs, Autophagy-related genes; MRGs, Metastasis-related genes; ssGSEA, Single-sample gene set enrichment analysis; DEGs, Differentially expressed genes; OS, Overall survival; LASSO, Least absolute shrinkage and selection operator; K-M, Kaplan-Meier; ROC, Receiver operating characteristic; AUC, Area under curve; DCA, Decision curve analysis; GSEA, Gene set enrichment analysis; GSVA, Gene set variation analysis; TIDE, Tumor Immune Dysfunction and Exclusion; CIBERSORT, The cell-type identification by estimating relative subsets Of RNATranscripts; SNP, Single-nucleotide polymorphism; TMB, Tumor mutation burden; WB, Western blotting; PVDF, Preactivated polyvinylidene difluoride; IHC, Immunohistochemistry; *SPP1*, Secreted phosphoprotein 1; *JCHAIN*, Joining chain of multimeric IgA and IgM; *DNASE1L3*, Deoxyribonuclease; *SNAI1*, Snail family transcriptional repressor 1; *TPM1*, Tropomyosin 1; *FKBP10*, *FKBP* prolyl isomerase 10; HAVCR2, Hepatitis A virus cellular receptor 2; LAG3, Lymphoctye activating 3; PDCD1, Programmed cell death 1; *CTLA-4*, Cytotoxic T lymphocyte antigen 4; *PDCD1*, Programmed cell death 1; *TIGIT*, T cell immunoreceptor with Ig and ITIM domains.

Data Sharing Statement

The datasets analyzed for this study can be found in the TCGA database (TCGA-COAD and TCGA-READ, https://portal.gdc.cancer.gov) and GEO database (GSE17536, GSE41568, GSE81558, GSE245552 and GSE178318, https://www.ncbi.nlm.nih.gov/geo/).

Ethics Approval and Consent to Participate

This study strictly adhered to the principles of the Declaration of Helsinki. The Second Affiliated Hospital of Wenzhou Medical University and Yuying Children's Hospital approved the conduct of this study within their institution (Ethics Approval Number: 2025-K-153-01). This study has obtained the informed consent of the patients, and their detailed pathological characteristics are summarized in Supplementary Table 4. This study is a population-based retrospective cohort study, and the TCGA and GEO databases used are all public data. Therefore, no additional informed consent was obtained from patients.

Author Contributions

All authors made a significant contribution to the work reported, whether that is in the conception, study design, execution, acquisition of data, analysis and interpretation, or in all these areas; took part in drafting, revising or critically reviewing the article; gave final approval of the version to be published; have agreed on the journal to which the article has been submitted; and agree to be accountable for all aspects of the work.

Funding

This work was supported by the Zhejiang Provincial Natural Science Foundation of China (No. LY20H160014), the Wenzhou Natural Science Research Foundation (No. Y20240298), and the Discipline Cluster of Oncology, Wenzhou Medical University, China (z2-2023013).

Disclosure

The authors report no conflicts of interest in this work.

References

1. Siegel RL, Kratzer TB, Giaquinto AN, Sung H, Jemal A. Cancer statistics, 2025. *CA Cancer J Clin*. 2025;75(1):10–45. doi:10.3322/caac.21871
2. Anbari K, Ghanadi K. Colorectal cancer: risk factors, novel approaches in molecular screening and treatment. *Int J Mol Cell Med*. 2025;14 (1):576–605. doi:10.22088/IJMCM.BUMS.14.1.576
3. Wu Y, He S, Cao M, et al. Comparative analysis of cancer statistics in China and the United States in 2024. *Chin Med J*. 2024;137(24):3093–3100. doi:10.1097/CM9.0000000000003442
4. Shinji S, Yamada T, Matsuda A, et al. Recent advances in the treatment of colorectal cancer: a review. *Jo Nippon Med School*. 2022;89(3):246–254. doi:10.1272/jnms.JNMS.2022_89-310
5. Ahmed M. Colon cancer: a clinician's perspective in 2019. *Gastroenterol Res*. 2020;13(1):1–10. doi:10.14740/gr1239
6. Siegel RL, Wagle NS, Cercek A, Smith RA, Jemal A. Colorectal cancer statistics. *CA Cancer J Clin*. 2023;73(3):233–254. doi:10.3322/caac.21772
7. Biller LH, Schrag D. Diagnosis and treatment of metastatic colorectal cancer: a review. *JAMA*. 2021;325(7):669–685. doi:10.1001/jama.2021.0106
8. Osei-Bordom DC, Kamarajah S, Christou N. Colorectal cancer, liver metastases and biotherapies. *Biomedicines*. 2021;9(8):894. doi:10.3390/biomedicines9080894
9. Jin Z, Li Y, Yi H, et al. Pathogenetic development, diagnosis and clinical therapeutic approaches for liver metastasis from colorectal cancer. *Int J Oncol*. 2025;66(3). doi:10.3892/ijo.2025.5728
10. Kong WS, Li JJ, Deng YQ, Ju HQ, Xu RH. Immunomodulatory molecules in colorectal cancer liver metastasis. *Cancer Lett*. 2024;598:217113. doi:10.1016/j.canlet.2024.217113
11. Ruff SM, Shannon AH, Pawlik TM. The role of targeted therapy in the multi-disciplinary approach to colorectal liver metastasis. *Cancers*. 2023;15 (13):3513. doi:10.3390/cancers15133513
12. Creasy JM, Sadot E, Koerkamp BG, et al. Actual 10-year survival after hepatic resection of colorectal liver metastases: what factors preclude cure? *Surgery*. 2018;163(6):1238–1244. doi:10.1016/j.surg.2018.01.004
13. Zhao L, Xi L, Liu Y, et al. The impact of tertiary lymphoid structures on tumor prognosis and the immune microenvironment in colorectal cancer. *Biomedicines*. 2025;13(3):539. doi:10.3390/biomedicines13030539
14. Dai S, Xu F, Xu X, et al. miR-455/GREM1 axis promotes colorectal cancer progression and liver metastasis by affecting PI3K/AKT pathway and inducing M2 macrophage polarization. *Cancer Cell Int*. 2024;24(1):235. doi:10.1186/s12935-024-03422-1
15. Safari MH, Rahimzadeh P, Alaei E, et al. Targeting ferroptosis in gastrointestinal tumors: interplay of iron-dependent cell death and autophagy. *Mol Cell Probes*. 2025;79:102013. doi:10.1016/j.mcp.2025.102013
16. Zhang Y, Li H, Lv L, et al. Autophagy: dual roles and perspective for clinical treatment of colorectal cancer. *Biochimie*. 2023;206:49–60. doi:10.1016/j.biochi.2022.10.004
17. Debnath J, Gammoh N, Ryan KM. Autophagy and autophagy-related pathways in cancer. *Nat Rev Mol Cell Biol*. 2023;24(8):560–575. doi:10.1038/s41580-023-00585-z
18. Zhao L, Zhang H, Wang S, et al. Hsa_circ_0000231 accelerates cell autophagy and promotes cell proliferation and invasion of colorectal cancer via miR-140-3p/Bcl-2 axis. *Mol Carcinog*. 2025;64(6):1025–1038. doi:10.1002/mc.23906
19. Li F, Wan X, Li Z, Zhou L. The NR3C2-SIRT1 signaling axis promotes autophagy and inhibits epithelial mesenchymal transition in colorectal cancer. *Cell Death Dis*. 2025;16(1):295. doi:10.1038/s41419-025-07575-3
20. Devenport SN, Singhal R, Radyk MD, et al. Colorectal cancer cells utilize autophagy to maintain mitochondrial metabolism for cell proliferation under nutrient stress. *JCI Insight*. 2021;6(14). doi:10.1172/jci.insight.138835
21. Bouznad N, Rokavec M, Öner MG, Hermeking H. Hermeking H. miR-34a and IRE1A/XBP-1(S) form a double-negative feedback loop to regulate hypoxia-induced emt, metastasis, chemo-resistance and autophagy. *Cancers*. 2023;15(4):1143. doi:10.3390/cancers15041143
22. Ni B, He X, Zhang Y, et al. Tumor-associated macrophage-derived GDNF promotes gastric cancer liver metastasis via a GFRA1-modulated autophagy flux. *Cell Oncol Dordr*. 2023;46(2):315–330. doi:10.1007/s13402-022-00751-z
23. He R, Wang M, Zhao C, et al. TFEB-driven autophagy potentiates TGF-β induced migration in pancreatic cancer cells. *J Exp Clin Cancer Res*. 2019;38(1):340. doi:10.1186/s13046-019-1343-4
24. Tian Y, Liang L, Chen J, et al. Knockdown LIMP2 inhibits colorectal cancer cells migration, invasion, and metastasis. *Exp Cell Res*. 2023;431 (1):113757. doi:10.1016/j.yexcr.2023.113757
25. Choi JH, Park SY, Lee WJ, et al. SEC22B inhibition attenuates colorectal cancer aggressiveness and autophagic flux under unfavorable environment. *Biochem Biophys Res Commun*. 2023;665:10–18. doi:10.1016/j.bbrc.2023.03.039
26. Dienstmann R, Vermeulen L, Guinney J, Kopetz S, Tejpar S, Tabernero J. Consensus molecular subtypes and the evolution of precision medicine in colorectal cancer. *Nat Rev Cancer*. 2017;17(4):268. doi:10.1038/nrc.2017.24
27. Mai D, Ding P, Tan L, et al. PIWI-interacting RNA-54265 is oncogenic and a potential therapeutic target in colorectal adenocarcinoma. *Theranostics*. 2018;8(19):5213–5230. doi:10.7150/thno.28001
28. Manfredi S, Lepage C, Hatem C, Coatmeur O, Faivre J, Bouvier AM. Epidemiology and management of liver metastases from colorectal cancer. *Ann Surg*. 2006;244(2):254–259. doi:10.1097/01.sla.0000217629.94941.cf

29. Chen Y, Chen Y, Zhang J, et al. Fusobacterium nucleatum promotes metastasis in colorectal cancer by activating autophagy signaling via the upregulation of CARD3 expression. *Theranostics*. 2020;10(1):323–339. doi:10.7150/thno.38870
30. Qu J, Chen Q, Bing Z, et al. C. tropicalis promotes CRC by down-regulating tumor cell-intrinsic PD-1 receptor via autophagy. *J Cancer*. 2023;14 (10):1794–1808. doi:10.7150/jca.79664
31. Kenific CM, Stehbens SJ, Goldsmith J, et al. NBR1 enables autophagy-dependent focal adhesion turnover. *J Cell Biol*. 2016;212(5):577–590. doi:10.1083/jcb.201503075
32. Sharifi MN, Mowers EE, Drake LE, et al. Autophagy promotes focal adhesion disassembly and cell motility of metastatic tumor cells through the direct interaction of paxillin with LC3. *Cell Rep*. 2016;15(8):1660–1672. doi:10.1016/j.celrep.2016.04.065
33. Liu W-Q, Li W-L, Ma S-M, Liang L, Kou Z-Y, Yang J. Discovery of core gene families associated with liver metastasis in colorectal cancer and regulatory roles in tumor cell immune infiltration. *Transl Oncol*. 2021;14(3):101011. doi:10.1016/j.tranon.2021.101011
34. Liu F, Song Z-M, Wang X-D, et al. Long non-coding RNA signature for liver metastasis of colorectal cancers. *Front Cell Dev Biol*. 2021;9:707115. doi:10.3389/fcell.2021.707115
35. Tang X-L, Xu Z-Y, Guan J, et al. Establishment of a neutrophil extracellular trap-related prognostic signature for colorectal cancer liver metastasis and expression validation of CYP4F3. *Clin Exp Med*. 2024;24(1):112. doi:10.1007/s10238-024-01378-0
36. Chen S, Wang Y, Wang B, et al. A signature based on 11 autophagy genes for prognosis prediction of colorectal cancer. *PLoS One*. 2021;16(10): e0258741. doi:10.1371/journal.pone.0258741
37. Zhao H, Huang C, Luo Y, et al. A correlation study of prognostic risk prediction for colorectal cancer based on autophagy signature genes. *Front Oncol*. 2021;11:595099. doi:10.3389/fonc.2021.595099
38. Zheng S, He H, Zheng J, et al. Machine learning-based screening and validation of liver metastasis-specific genes in colorectal cancer. *Sci Rep*. 2024;14(1):17679. doi:10.1038/s41598-024-68706-y
39. Omran TA, Tunsjø HS, Jahanlu D, Brackmann SA, Bemanian V, Sæther PC. Decoding immune-related gene-signatures in colorectal neoplasia. *Front Immunol*. 2024;15:1407995. doi:10.3389/fimmu.2024.1407995
40. Kumbrink J, Bohlmann L, Mamlouk S, et al. Serial analysis of gene mutations and gene expression during first-line chemotherapy against metastatic colorectal cancer: identification of potentially actionable targets within the multicenter prospective biomarker study reveal. *Cancers*. 2022;14(15):3631. doi:10.3390/cancers14153631
41. Liu X, Qin J, Nie J, et al. ANGPTL2+cancer-associated fibroblasts and SPP1+macrophages are metastasis accelerators of colorectal cancer. *Front Immunol*. 2023;14:1185208. doi:10.3389/fimmu.2023.1185208
42. Zhou J, Song Q, Li H, et al. Targeting circ-0034880-enriched tumor extracellular vesicles to impede SPP1highCD206+ pro-tumor macrophages mediated pre-metastatic niche formation in colorectal cancer liver metastasis. *Mol Cancer*. 2024;23(1):168. doi:10.1186/s12943-024-02086-9
43. Zhu W-Z, Feng D-C, Xiong Q, et al. An autophagy-related gene prognostic index predicting biochemical recurrence, metastasis, and drug resistance for prostate cancer. *Asian J Androl*. 2023;25(2):208–216. doi:10.4103/aja202281
44. Li T, Zhang L. Autophagy-related biomarkers in hepatocellular carcinoma and their relationship with immune infiltration. *Discov Oncol*. 2024;15 (1):299. doi:10.1007/s12672-024-01167-x
45. Dong B, Wu Y. Epigenetic regulation and post-translational modifications of SNAI1 in cancer metastasis. *Int J Mol Sci*. 2021;22(20):11062. doi:10.3390/ijms222011062
46. Pavlič A, Hauptman N, Boštjančič E, Zidar N. Long non-coding RNAs as potential regulators of EMT-related transcription factors in colorectal cancer-a systematic review and bioinformatics analysis. *Cancers*. 2022;14(9):2280. doi:10.3390/cancers14092280
47. Zhang X, Luo Y, Cen Y, et al. MACC1 promotes pancreatic cancer metastasis by interacting with the EMT regulator SNAI1. *Cell Death Dis*. 2022;13(11):923. doi:10.1038/s41419-022-05285-8
48. Zhang Y, Tan Y, Yuan J, et al. circLIFR-007 reduces liver metastasis via promoting hnRNPA1 nuclear export and YAP phosphorylation in breast cancer. *Cancer Lett*. 2024;592:216907. doi:10.1016/j.canlet.2024.216907
49. Zada S, Hwang JS, Ahmed M, Lai TH, Pham TM, Kim DR. Control of the epithelial-to-mesenchymal transition and cancer metastasis by autophagy-dependent SNAI1 degradation. *Cells*. 2019;8(2):129. doi:10.3390/cells8020129
50. Grassi G, Di Caprio G, Santangelo L, et al. Autophagy regulates hepatocyte identity and epithelial-to-mesenchymal and mesenchymal-to-epithelial transitions promoting snail degradation. *Cell Death Dis*. 2015;6(9):e1880. doi:10.1038/cddis.2015.249
51. Pang M, Wang H, Rao P, et al. Autophagy links β-catenin and Smad signaling to promote epithelial-mesenchymal transition via upregulation of integrin linked kinase. *Int J Biochem Cell Biol*. 2016;76:123–134. doi:10.1016/j.biocel.2016.05.010
52. Hwang JS, Lai TH, Ahmed M, et al. Regulation of TGF-β1-induced EMT by autophagy-dependent energy metabolism in cancer cells. *Cancers*. 2022;14(19):4845. doi:10.3390/cancers14194845
53. Xie M, Liang L, Yu L, et al. The integration of bulk and single-cell sequencing data revealed the function of FKBP10 in the gastric cancer microenvironment. *Transl Cancer Res*. 2024;13(2):975–988. doi:10.21037/tcr-23-1484
54. Chen Z, He L, Zhao L, et al. circREEP3 drives colorectal cancer progression via activation of FKBP10 transcription and restriction of antitumor immunity. *Adv Sci*. 2022;9(13):e2105160. doi:10.1002/advs.202105160
55. Sun Z, Qin X, Fang J, Tang Y, Fan Y. Multi-omics analysis of the expression and prognosis for FKBP gene family in renal cancer. *Front Oncol*. 2021;11:697534. doi:10.3389/fonc.2021.697534
56. Shen C, Yan Y, Yang S, et al. Construction and validation of a bladder cancer risk model based on autophagy-related genes. *Funct Integr Genomics*. 2023;23(1):46. doi:10.1007/s10142-022-00957-2
57. Shen K, Ke S, Chen B, et al. Identification and validation of biomarkers for epithelial-mesenchymal transition-related cells to estimate the prognosis and immune microenvironment in primary gastric cancer by the integrated analysis of single-cell and bulk RNA sequencing data. *Math Biosci Eng*. 2023;20(8):13798–13823. doi:10.3934/mbe.2023614
58. Li H, Pan L, Guo J, Lao J, Wei M, Huang F. Integration of single-cell and bulk RNA sequencing to establish a prognostic signature based on tumor-associated macrophages in colorectal cancer. *BMC Gastroenterol*. 2023;23(1):385. doi:10.1186/s12876-023-03035-4
59. Liu J, Yi J, Zhang Z, Cao D, Li L, Yao Y. Deoxyribonuclease 1-like 3 may be a potential prognostic biomarker associated with immune infiltration in colon cancer. *Aging*. 2021;13(12):16513–16526. doi:10.18632/aging.203173
60. Li W, Nakano H, Fan W, et al. DNASE1L3 enhances antitumor immunity and suppresses tumor progression in colon cancer. *JCI Insight*. 2023;8 (17). doi:10.1172/jci.insight.168161

61. Mlakar V, Berginc G, Volavsek M, Stor Z, Rems M, Glavac D. Presence of activating KRAS mutations correlates significantly with expression of tumour suppressor genes DCN and TPM1 in colorectal cancer. *BMC Cancer*. 2009;9(1):282. doi:10.1186/1471-2407-9-282
62. Li C, Hong S, Hu H, Liu T, Yan G, Sun D. MYC-induced upregulation of lncrna ELFN1-AS1 contributes to tumor growth in colorectal cancer via epigenetically silencing TPM1. *Mol Cancer Res*. 2022;20(11):1697–1708. doi:10.1158/1541-7786.MCR-22-0009
63. Liang W, Wu J, Qiu X. LINC01116 facilitates colorectal cancer cell proliferation and angiogenesis through targeting EZH2-regulated TPM1. *J Transl Med*. 2021;19(1):45. doi:10.1186/s12967-021-02707-7
64. Wei J, Chen Z, Hu M, et al. Characterizing intercellular communication of pan-cancer reveals SPP1+ tumor-associated macrophage expanded in hypoxia and promoting cancer malignancy through single-cell RNA-seq data. *Front Cell Dev Biol*. 2021;9:749210. doi:10.3389/fcell.2021.749210
65. Zhou M, Li R, Lian G, et al. Tetrahydrocurcumin alleviates colorectal tumorigenesis by modulating the SPP1/CD44 axis and preventing M2 tumor-associated macrophage polarization. *Phytomedicine*. 2025;141:156674. doi:10.1016/j.phymed.2025.156674
66. Xie Z, Zheng G, Niu L, et al. SPP1 macrophages in colorectal cancer: markers of malignancy and promising therapeutic targets. *Genes Dis*. 2025;12(3):101340. doi:10.1016/j.gendis.2024.101340
67. Lee J-A, Park HE, Lee D-W, et al. Immunogenomic characteristics and prognostic implications of terminally exhausted CD8+ T cells in colorectal cancers. *Front Immunol*. 2025;16:1601188. doi:10.3389/fimmu.2025.1601188
68. Waldman AD, Fritz JM, Lenardo MJ. A guide to cancer immunotherapy: from T cell basic science to clinical practice. *Nat Rev Immunol*. 2020;20 (11):651–668. doi:10.1038/s41577-020-0306-5
69. Huang S, Xu J, Baran N, Ma W. Advancing the next generation of cancer treatment with circular RNAs in CAR-T cell therapy. *Biomed Pharmacother*. 2024;181:117753. doi:10.1016/j.biopha.2024.117753
70. Huang H, Ge J, Fang Z, et al. Precursor exhausted CD8+T cells in colorectal cancer tissues associated with patient's survival and immunotherapy responsiveness. *Front Immunol*. 2024;15:1362140. doi:10.3389/fimmu.2024.1362140
71. Wu H, Fan P-W, Feng Y-N, et al. Role of T cell exhaustion and tissue-resident memory T cells in the expression and prognosis of colorectal cancer. *Sci Rep*. 2025;15(1):28503. doi:10.1038/s41598-025-14409-x
72. Ling T, Zhang C, Liu Y, Jiang C, Gu L. Single-cell analysis revealed a potential role of T-cell exhaustion in colorectal cancer with liver metastasis. *J Cell Mol Med*. 2024;28(8):e18341. doi:10.1111/jcmm.18341
73. Silinskaite U, Valciukiene J, Jakubauskas M, Poskus T. The immune environment in colorectal adenoma: a systematic review. *Biomedicines*. 2025;13(3):699. doi:10.3390/biomedicines13030699
74. Cancro MP, Tomayko MM. Memory B cells and plasma cells: the differentiative continuum of humoral immunity. *Immunol Rev*. 2021;303 (1):72–82. doi:10.1111/imr.13016
75. Yi M, Li T, Niu M, et al. Exploiting innate immunity for cancer immunotherapy. *Mol Cancer*. 2023;22(1):187. doi:10.1186/s12943-023-01885-w
76. Cao L, Dai H, Wei S, et al. Endoplasmic reticulum stress-related prognosis signature characterizes the immune landscape and predicts the prognosis of colon adenocarcinoma. *Front Genet*. 2025;16:1516232. doi:10.3389/fgene.2025.1516232
77. Zhang TA, Zhang Q, Zhang J, et al. Identification of the role of endoplasmic reticulum stress genes in endometrial cancer and their association with tumor immunity. *BMC Med Genomics*. 2023;16(1):261. doi:10.1186/s12920-023-01679-5
78. Huang L, Wang Z, Chang Y, et al. EFEMP2 indicates assembly of M0 macrophage and more malignant phenotypes of glioma. *Aging*. 2020;12 (9):8397–8412. doi:10.18632/aging.103147
79. Liu X, Wang X, Zhang J, et al. Myc-mediated inhibition of HIF1a degradation promotes M2 macrophage polarization and impairs CD8 T cell function through lactic acid secretion in ovarian cancer. *Int Immunopharmacol*. 2024;141:112876. doi:10.1016/j.intimp.2024.112876
80. Chang CP, Hu MH, Hsiao YP, Wang YC. ST2 signaling in the tumor microenvironment. *Adv Exp Med Biol*. 2020;1240:83–93.
81. Lai Y-S, Wahyuningtyas R, Aui S-P, Chang K-T. Autocrine VEGF signalling on M2 macrophages regulates PD -L1 expression for immunomodulation of T cells. *J Cell Mol Med*. 2019;23(2):1257–1267. doi:10.1111/jcmm.14027
82. Liu M, Wei F, Wang J, et al. Myeloid-derived suppressor cells regulate the immunosuppressive functions of PD-1−PD-L1+ Bregs through PD-L1 /PI3K/AKT/NF-κB axis in breast cancer. *Cell Death Dis*. 2021;12(5):465. doi:10.1038/s41419-021-03745-1
83. Joshi S, Sharabi A. Targeting myeloid-derived suppressor cells to enhance natural killer cell-based immunotherapy. *Pharmacol Ther*. 2022;235:108114. doi:10.1016/j.pharmthera.2022.108114
84. Fu J, Li K, Zhang W, et al. Large-scale public data reuse to model immunotherapy response and resistance. *Genome Med*. 2020;12(1):21. doi:10.1186/s13073-020-0721-z
85. Yoo S-A, Leng L, Kim B-J, et al. MIF allele-dependent regulation of the MIF coreceptor CD44 and role in rheumatoid arthritis. *Proc Natl Acad Sci U S A*. 2016;113(49):E7917–e26. doi:10.1073/pnas.1612717113
86. Cabrero-de Las Heras S, Martínez-Balibrea E. CXC family of chemokines as prognostic or predictive biomarkers and possible drug targets in colorectal cancer. *World J Gastroenterol*. 2018;24(42):4738–4749. doi:10.3748/wjg.v24.i42.4738
87. Acharyya S, Oskarsson T, Vanharanta S, et al. A CXCL1 paracrine network links cancer chemoresistance and metastasis. *Cell*. 2012;150 (1):165–178. doi:10.1016/j.cell.2012.04.042
88. Kasashima H, Yashiro M, Nakamae H, et al. Clinicopathologic significance of the CXCL1-CXCR2 axis in the tumor microenvironment of gastric carcinoma. *PLoS One*. 2017;12(6):e0178635. doi:10.1371/journal.pone.0178635
89. Wang H, Zhang B, Li R, et al. KIAA1199 drives immune suppression to promote colorectal cancer liver metastasis by modulating neutrophil infiltration. *Hepatology*. 2022;76(4):967–981. doi:10.1002/hep.32383
90. Zamani B, Ramazani A, Saberzadeh J, Rostampour P, Takhshid MA. The effect of annexin A5 overexpression on invasiveness and expression of the genes involved in epithelial-mesenchymal transition of HCT 116 cell line. *Mol Biol Res Commun*. 2023;12(2):77–85. doi:10.22099/mbrc.2023.47160.1823
91. Rocha MR, Morgado-Diaz JA. Epithelial-mesenchymal transition in colorectal cancer: annexin A2 is caught in the crosshairs. *J Cell Mol Med*. 2021;25(22):10774–10777. doi:10.1111/jcmm.16962
92. Lu X, Hu L, Mao J, Zhang S, Cai Y, Chen W. Annexin A9 promotes cell proliferation by regulating the Wnt signaling pathway in colorectal cancer. *Hum Cell*. 2023;36(5):1729–1740. doi:10.1007/s13577-023-00939-x

ImmunoTargets and Therapy

Dovepress
Taylor & Francis Group

Publish your work in this journal

ImmunoTargets and Therapy is an international, peer-reviewed open access journal focusing on the immunological basis of diseases, potential targets for immune based therapy and treatment protocols employed to improve patient management. Basic immunology and physiology of the immune system in health, and disease will be also covered. In addition, the journal will focus on the impact of management programs and new therapeutic agents and protocols on patient perspectives such as quality of life, adherence and satisfaction. The manuscript management system is completely online and includes a very quick and fair peer-review system, which is all easy to use. Visit http://www.dovepress.com/testimonials.php to read real quotes from published authors.

Submit your manuscript here: http://www.dovepress.com/immunotargets-and-therapy-journal